



Southernmost Kerguelen Plateau – Not a continental fragment

Wilfried Jokat^{a,b,*}, Tabea Altenbernd-Lang^a, Karsten Gohl^a, German L. Leitchenkov^{c,d}, Hannes Eisermann^a

^a Alfred Wegener Institute, Helmholtz Centre for Polar and Marine Research, Am Alten Hafen 26, 27568 Bremerhaven, Germany

^b University of Bremen, Geoscience Department, Klagenfurter Str. 4, 28359 Bremen, Germany

^c All-Russia Scientific Research Institute for Geology and Mineral Resources of the Ocean, Angliiskii pr. 1, St.-Petersburg 190121, Russia

^d Institute of Earth Sciences, Saint Petersburg State University, Universitetskaya nab. 7-9, 199034 St.-Petersburg, Russia

ARTICLE INFO

Keywords:

Marine geophysical and geological research
Geodynamics
Tectonophysics
Deep seismic sounding
Oceanic and Continental crustal composition
Gravity modelling

ABSTRACT

Most models on the early continental drift of the Indian continent from Antarctica are guided by the existence of microcontinents that are supposed to be located beneath Elan Bank and the Southern Kerguelen Plateau in the Enderby Basin off East Antarctica. Two deep seismic lines were acquired to test these ideas by investigating the distribution of oceanic and continental crust in the Enderby Basin. In this contribution, we discuss the results of the eastern profile which images the crustal structure of the southernmost Kerguelen Plateau. The new deep seismic data show that the seismic velocity structure of the southernmost Kerguelen Plateau is different to that of extended continental crust but similar to other igneous oceanic plateaus worldwide. At the northern end of the profile, the Moho discontinuity lies at a depth below sea level of approximately 25 km. The position of the East Antarctic continent-ocean boundary is located close to its continental shelf edge. The maximum thickness of the East Antarctic transitional crust, at the southern termination of our line, is 22 km. Extrapolating our seismic reflection and refraction results show that the oceanic crust at 50° - 90°E in the Enderby Basin and Princess Elizabeth Trough formed whilst in receipt of excess melt from the Kerguelen plume around magnetic chron M4n causing a northward thickening of the oceanic crust since 130 Ma. These results strongly support a one-phase model for the drift of the Indian plate.

1. Introduction

The crustal affinity of the gigantic volcanic Kerguelen Plateau in the Indian Ocean sector of East Antarctica (Fig. 1) and its role in the continental breakup between India and Antarctica is subject of this study. While five scientific drilling expeditions (see Coffin et al., 2002 for an overview) have provided reasonably good control on the eruption history of the plateau, none of them provided direct constraints on the composition of the crust beneath the basalts that make up the top surface of its basement. Indirectly, however, geophysical and geochemical constraints have been taken to suggest a two-phase model for the separation of the Indian and Antarctic plates, in which parts of the plateau are assumed to comprise microcontinents that became stranded in the transition between the two phases as the plate boundary shifted northwards (Gaina et al., 2007; see next chapter). However, as geochemical rock analyses have only a limited potential to constrain the composition of the deeper crust of oceanic plateaus (Class and Le Roex, 2011) and the

interpretation of unequally distributed/spaced magnetic profiles in the oceanic basins surrounding the plateau is difficult, the model remained speculative. Seismic wide-angle data on the crustal compositions of the Enderby Land margin and its conjugate, the southernmost tip of the Southern Kerguelen Plateau (SKP), were missing to constrain the interpretation of the potential field data. In 2007 and 2012, this knowledge gap was closed by the acquisition of seismic wide-angle and magnetic data along two profiles in the Enderby Basin and the Princess Elizabeth Trough. Their interpretation made it necessary to reject the two-phase model (Jokat et al., 2021). One of these lines was located across the Princess Elizabeth Trough (PET; Fig. 1; AWI-20070200). In addition to Jokat et al. (2021), we present and discuss the complete details of the seismic modelling/raytracing as well as a 2D density model. Furthermore, we compare and discuss our velocity-depth functions with results from other regions to support our interpretation. Finally, by using the existing seismic reflection and refraction profiles across the East Antarctic margin in our research area, we extend the continent-ocean

* Corresponding author at: Alfred Wegener Institute, Helmholtz Centre for Polar and Marine Research, Am Alten Hafen 26, 27568 Bremerhaven, Germany.
E-mail address: Wilfried.Jokat@awi.de (W. Jokat).

<https://doi.org/10.1016/j.tecto.2025.230804>

Received 2 December 2024; Received in revised form 20 May 2025; Accepted 26 May 2025

Available online 27 May 2025

0040-1951/© 2025 The Authors. Published by Elsevier B.V. This is an open access article under the CC BY license (<http://creativecommons.org/licenses/by/4.0/>).

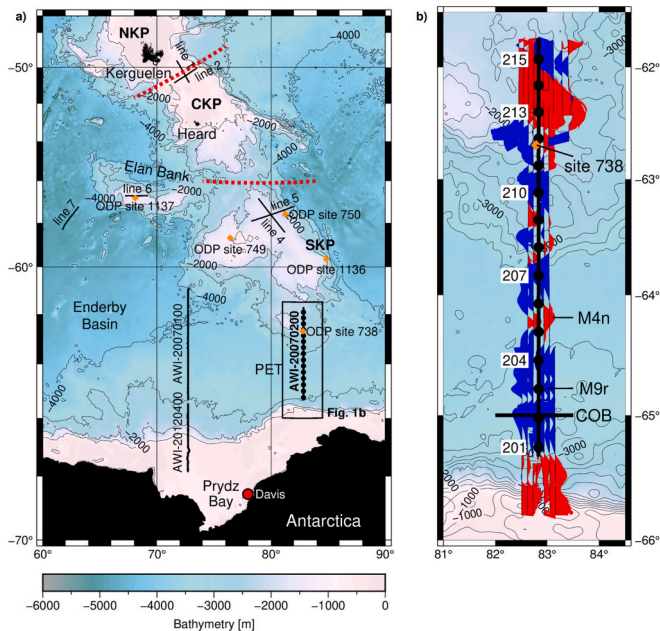


Fig. 1. (a) Overview of the East Antarctic margin and Kerguelen Plateau showing the deep seismic wide-angle/refraction lines AWI-20070100, AWI-20120400 (Altenbernd-Lang et al., 2022) and AWI-20070200 (this study), the ODP drill sites on the Southern Kerguelen Plateau and Elan Bank as well as pre-existing MD66/KeOBS cruise seismic wide-angle/refraction lines labelled lines 1–7 (Operto and Charvis, 1995; Borissova et al., 2003). The orange dotted lines indicate the approximate boundaries between the Northern, Central, and Southern Kerguelen Plateau (Coffin et al., 2002). The position of the Australian Antarctic Davis Station is marked by a red dot. The distance between the station and the southernmost OBS is approx. 450 km. Bathymetric contour lines have a spacing of 1000 m. Abbreviations: NKP – Northern Kerguelen Plateau, PET – Princess Elizabeth Trough, SKP – Southern Kerguelen Plateau, CKP – Central Kerguelen Plateau,

(b) OBS/OBH station locations 201–215 of profile AWI-20070200 and amplitude display of helicopter magnetic tracks acquired parallel to the seismic profile with their identified chrons M9r to M4n (Cande and Kent, 1995; Gradstein et al., 2004; Jokat et al., 2021). COB annotates the interpreted continent-ocean boundary. Bathymetric contour lines have a spacing of 250 m. (For interpretation of the references to colour in this figure legend, the reader is referred to the web version of this article.)

boundary (COB) location of Altenbernd-Lang et al. (2022) for the Enderby Basin into the Princess Elizabeth Trough.

1.1. Geological and geophysical knowledge

The southern supercontinent Gondwana, consisting of the modern continents South America, Africa, India/Madagascar, Australia, and Zealandia, with Antarctica in its center, started to disintegrate in the Early Jurassic. Onshore geological mapping and rock dating indicate that massive volcanism started around 184 Ma in the Chon Aike province located in southern South America (Pankhurst and Rapela, 1995), and around 183 Ma in the Karoo-Ferrar province of Dronning Maud Land (Antarctica) and southern East Africa (e.g. Jourdan et al., 2007). The formation of oceanic crust started some time after this initial magmatic pulse. The oldest magnetic seafloor spreading anomalies in the Weddell Sea and off Dronning Maud Land and their conjugate areas allow to reconstruct the northwards drift of South America and Africa since approximately 165 Ma (e.g. Jokat et al., 2003; König and Jokat, 2006; Müller and Jokat, 2019; Eagles and Eisermann, 2020). After the breakup of South America and Africa from Antarctica, the dispersal of the remaining southern continents continued further east at about 133 Ma, with the formation of new oceanic crust in the Enderby Basin and the Davis Sea as Sri Lanka, India and Madagascar detached (Jokat et al.,

2021). Remarkably, this phase was not accompanied by massive onshore volcanism similar to the Karoo-Ferrar large igneous province in Antarctica (Lisker, 2004). Simultaneously, the Indian plate separated from West Australia. This is well documented in the Perth Abyssal Plain off West Australia (PAP), where the oldest spreading anomaly has formed during chron M9 (Gibbons et al., 2012; Williams et al., 2013). In contrast to the Enderby Basin, the PAP hosts a well-defined extinct spreading axis (Dirk Hartog Ridge, Williams et al., 2013) in its center. Seaward, the PAP is rimmed by two continental fragments, the Gulden Draak and Batavia knolls (Gibbons et al., 2012; Williams et al., 2013). Both observations document a ridge jump approximately between 101 and 103 Ma between the Indian and Australian plates during their separation. Finally, the last two plates started to move northwards, Australia (e.g., Whittaker et al., 2013, 84 Ma; Eagles, 2019; <58 Ma) and Zealandia (e.g. Wobbe et al., 2012, 84 Ma), leaving the Antarctic plate behind in its polar position. Thus, Antarctica is the only part of Gondwana to have shared plate boundaries with today's other southern hemisphere plates.

In this contribution, we focus on the nature of southernmost South Kerguelen Plateau and its relationship with early drift of India, Sri Lanka, and Madagascar, which we refer to in this study as components of the Indian plate. The understanding of the initial drift of the Indian plate relative to East Antarctica has been debated for decades. Early geodynamic and plate-kinematic models for the separation of the two proposed continuous northward movement of the Indian plate at a stable single plate boundary, and the subsequent eruption of the Kerguelen Plateau onto its Antarctic flank, based on few and randomly distributed marine magnetic data off East Antarctica and East India (Patriat and Segoufin, 1988; Powell et al., 1988; Royer and Coffin, 1992; Nogi et al., 1996; Lawver et al., 1998; Ramana et al., 2001). As more magnetic data became available over time, newer compilations showed a pronounced positive magnetic anomaly, named the MacRobertson Coast Anomaly (MCA, Gaina et al., 2007) or Enderby Basin Anomaly (Golynsky et al., 2007), in the center of the Enderby Basin. This anomaly is located above a pronounced basement high imaged by seismic reflection data (Stagg et al., 2004; Leitchenkov et al., 2015). These observations, together with the absence of clearly identifiable seafloor spreading anomalies south of this strong magnetic anomaly, guided geodynamic models to propose it marked the position of the East Antarctic continent-ocean boundary (COB). This interpretation implied the presence of up to 450 km of thinned continental crust offshore of the Antarctic coastline. Analyses of drilled basaltic rocks on Elan Bank revealed some continental lithospheric components, and clasts of gneiss similar to rocks known from eastern India, led to inferences that the bank itself, and perhaps the neighboring Southern Kerguelen Plateau, are underlain by continental crust. Both were declared, by some authors, to form the conjugate continental rifted margins to Antarctica (Weis et al., 2001; Borissova et al., 2003; Gaina et al., 2007). The existing marine magnetic data were consequently reassessed, leading to suggestions of the presence of M-series (>126 Ma) isochrons north of the strong magnetic anomaly (Golynsky et al., 2007), in support of a two-phase geodynamic model in which the Elan Bank and Southern Kerguelen Plateau first detached from Antarctica together with India, and later after a ridge jump detached from India. This narrative requires the existence of an extinct spreading axis, an abandoned remnant of the first phase, somewhere south of the microcontinents in the Enderby Basin (Gaina et al., 2007).

The Kerguelen Plateau is the world's second largest submarine volcanic plateau by area (Coffin and Eldholm, 1994). Newly acquired magnetic data show that the oceanic crust south of the plateau in Princess Elizabeth Trough (PET) started to form at about 133 Ma (Jokat et al., 2021). The southernmost tip of the SKP is capped by basalts that erupted at ~120–105 Ma, as revealed by cored rocks from several scientific Ocean Drilling Program (ODP) legs (Royer and Coffin, 1992; Frey et al., 2002, 2003). The southernmost samples, closest to our profile, (Fig. 1) provided an $^{40}\text{Ar}/^{39}\text{Ar}$ age of 113 ± 3.5 Ma at ODP Leg 119 Site 738 (Coffin et al., 2002; Jiang et al., 2021). While these drilling

campaigns provided excellent constraints on the evolution of the Kerguelen Plateau, little is known about the volume of the erupted material before the Kerguelen Plateau formed due to the missing deep seismic profiles.

Deep seismic refraction lines acquired during N/O Marion Dufresne 66/KeOBS (MD66) cruise (Fig. 1; Operto and Charvis, 1996) provided the first insight on the thickness of the igneous crust of the Northern Kerguelen and Heard Plateau (Fig. 1; NKP/CKP; 23 km), the southern Kerguelen Plateau (Fig. 1; SKP; 22–23 km) around ODP Leg 119 drill sites 748, 749, and 750, and Elan Bank (up to 18 km) (Fig. 1). In 2007 and 2012, these surveys were supplemented by three deep seismic wide-angle/refraction lines, all accompanied by multiple parallel and coincident magnetic anomaly profiles, suitable for mapping the crustal fabric of the plateau's southern oceanic basins, the Enderby Basin and PET, flanking the SKP. The seismic lines start at the Antarctic continental margin and terminate north of it close to 68°S and 66°S (Hubberten, 2008; Jokat et al., 2021; Altenbernd-Lang et al., 2022). The congruent western profiles AWI-20070100 and AWI-20120400 (Fig. 1) aimed to investigate the crust between the Antarctic continental shelf and the MacRobertson Coast/Enderby Land magnetic anomaly, deep in the Enderby Basin. The objective of the profiles was to examine whether an extinct spreading axis exists, and to document the geometries (width, composition) of the continent-ocean transition and oceanic crust in the basin (Jokat et al., 2021; Altenbernd-Lang et al., 2022). The major findings were: (a) the MacRobertson Coast/Enderby Basin anomaly does not represent the COB, but instead is the signal of magnetic chron M4n developed over a basement high of variable height; (b) the COB is located about 160 km to the south of the anomaly (Altenbernd-Lang et al., 2022); (c) additional magnetic reversal isochrons are present south of M4n, reaching back as far as chron M9r and helping to constrain the COB; (d) north of chron M4n, the oceanic crust thickens to as much as 10 km, indicating the accommodation of increasing voluminous melt from the Kerguelen plume during its formation; and (f) there is no indication for the presence of an extinct spreading axis in the Princess Elizabeth Trough as extrapolated by Gaina et al. (2007) from their interpretation of the seismic and magnetic data in the central Enderby Basin.

1.1.1.1. Methods and modelling

Thirteen Lobster ocean-bottom seismometer (OBS) and 2 ocean-bottom hydrophone (OBH) systems manufactured by KUM, Kiel (<https://www.kum-kiel.de/about.html>) were deployed along the seismic wide-angle/refraction line AWI-20070200 (Fig. 1) (for more technical details, see Hubberten, 2008). The OBS/OBH spacing along the ~400 km long profile was approximately 27 km. The OBH stations were equipped only with a hydrophone, while the OBS stations additionally carried a 3-component 60-s broadband seismometer. In total, three channels for seismometer input and one for hydrophone signals were digitized by a Geolon MCS 24 bit data logger. The sampling frequency during the data acquisition was set to 250 Hz for all stations. The gain of the OBS hydrophones was set to 16, the gain of all seismometer channels (x,y,z) was set to 4. The gain of the OBH hydrophones was set to 5. The internal clocks of the recorders were synchronized with the external GPS time both before the deployments and after the recoveries of the stations (Altenbernd-Lang et al., 2022).

A cluster of 8 G-Guns (8.5 l volume each) with a total volume of 68 l, together with a single BOLT™ airgun (32.8 l volume), were used as seismic source. The shot interval was set to one minute, equivalent to an approximate shot distance of 150 m. Two of the G-Guns malfunctioned during the acquisition of the profile.

All 15 OBH/OBS were successfully recovered. After recovery, the internal drifts of the recorders (skew) were corrected based on the synchronization to GPS times before deployment and after recovery. A linear correction for the clock drift was applied to the seismic data. The OBS and OBH positions were checked by using the travel times of the direct water waves. If necessary, their positions were corrected so that

the apex of the direct water wave is symmetrical around an OBS/OBH deployment position.

For modelling of the sediments and the morphology of the oceanic crust, we used the Russian multichannel seismic reflection profile RAE39–10, acquired by the RV Akademik A. Karpinsky in 1994 (Fig. 2). All seismic reflection data used in this study were downloaded from the Antarctic Seismic Data Library System (SDLS).

1.1.1.1. Seismic analysis and modelling. We used the software *zp* (developed by Barry Zelt, see <http://www.soest.hawaii.edu/users/bzelt/>) for picking the refracted and reflected phases. Because of partly noisy seismometer channels, the hydrophone channels were used for picking most of the station records (Figs. 3–8). We applied a band-pass filter of 4–15 Hz to the data.

A ~ 400 km-long P-wave velocity model was obtained by forward modelling with the software *rayinvr* (Zelt and Smith, 1992) and the graphical interface *PRay* (Fromm, 2016). For the starting model, we used bathymetric data collected during the seismic acquisition, and basement topography extracted from an already existing seismic reflection profile RAE39–10 (Fig. 2).

Picked and raytraced travel times, the ray coverage of the refracted and reflected phases and the final velocity model are shown in Figs. 9–11.

1.1.1.1.1. Sediment layers. Three seismic refraction phases from the sedimentary cover were identified in the dataset and used to model the thicknesses and velocities of the sediment layers. Although only three sediment refraction phases were identified in the dataset, the maximum 3.5 km thick sediment package had to be modelled with up to four layers along the line (Figs. 3–8, 11). In the southern part of the model, the velocities of the uppermost sediment layer, are not constrained by any refracted phases. Their first arrivals are probably obscured by arrivals of the direct wave (P_w). As we could not pick any first arrivals for this layer, it is called P_{sed0} in the following. Three refracted phases from sedimentary layers, named P_{sed1} to P_{sed3} , are visible in many stations and have minimum/maximum velocities of $1.8\text{--}2.1 \pm 0.1$ km/s, $2.6\text{--}3.0 \pm 0.1$ km/s, and $3.0\text{--}3.4 \pm 0.1$ km/s at their tops and bases. Reflections marking the base of sediment layers 1, 2 and 3 are present in the PET ($P_{sed1}P$ to $P_{sed3}P$, Figs. 3, 4). Various basement reflections are visible in many records (e.g. Figs. 3, 10). Towards the SKP, at the northern part of the profile, the number of sediment layers was reduced to one, as the seismic reflection data show that the sediment cover thins significantly (Figs. 5–8). Here, the velocities of the uppermost sediment layer, P_{sed1} , are not constrained by any refracted phases. They are probably also obscured by arrivals of the direct wave (P_w). However, reflections from the base of the top sediment layer marking the top of basement north of the PET are visible in the data from stations 209–213 (Figs. 5–7, Fig. 10, $P_{sed1}P$).

1.1.1.1.1.1. Crustal layers and upper mantle

We identified four different crustal refracted phases, P_{c1} to P_{c4} . In the northern part of the model, the crust consists of up to four layers (Figs. 5–8). Here, refracted phases in the upper layer have velocities of $3.6\text{--}4.2 \pm 0.1$ km/s at its top and $4.2\text{--}4.8 \pm 0.1$ km/s at its base (Fig. 11a). The thickness of the layer varies (0–2.5 km). In the second (0.0–2.7 km thick) crustal layer, the refracted phases P_{c2} have a velocity of $5.0\text{--}5.4 \pm 0.1$ km/s. The base of the second crustal layer is constrained by some reflection phases ($P_{c2}P$, Fig. 8). In the SKP area, the underlying third crustal layer has a largely constant thickness of 2 km below the SKP, which increases to 4 km towards the PET. Refracted phases (P_{c3}) were modelled with velocities of $5.7\text{--}6.2 \pm 0.1$ km/s. The lowermost crustal layer below the SKP has a maximum thickness of 17 km and thins out towards the PET. Ray coverage of refracted arrivals is only achieved in its upper part, where the phases have a velocity of $6.7\text{--}6.8 \pm 0.2$ km/s (Figs. 6–8, 10, P_{c4}). Moho reflections (P_mP) constraining the base of this layer are visible in many records (Figs. 5–8, and supplementary material).

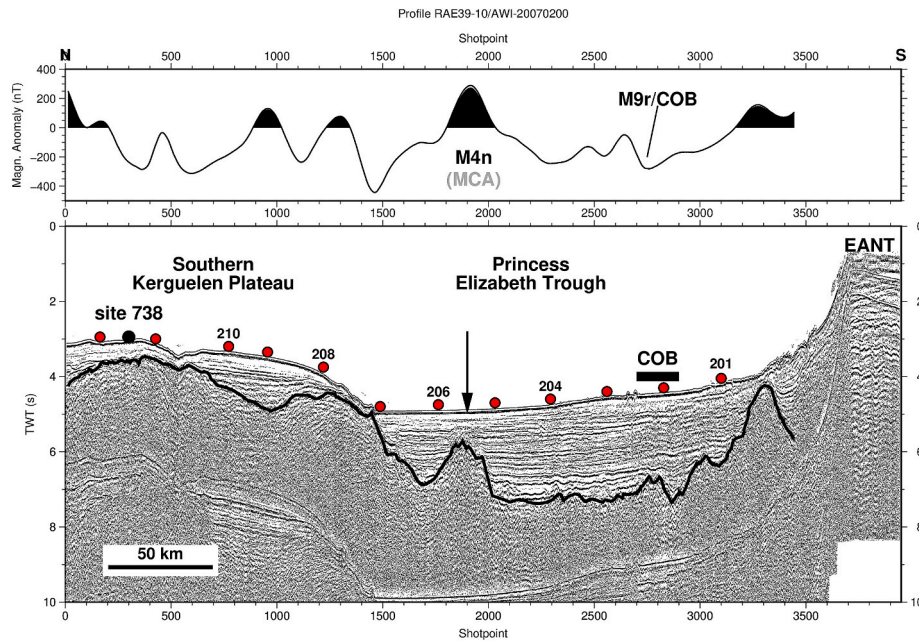


Fig. 2. Russian stacked seismic reflection line RAE39–10 across the PET (Leitchenkov et al., 2019). The location of the ~340 km long line is identical with the deep seismic wide-angle/refraction line presented in this paper. Upper panel: helicopter borne magnetic data acquired along a line closest to RAE39–10. The red dots mark the position of the OBS, which were deployed along the previously existing seismic reflection profile. Please note that this profile is approx. 60 km shorter than the seismic refraction profile. Thus, the positions of the northernmost three OBS (OBS213–215) are not displayed. The black dot marks ODP Site 738. MCA (darkgrey) and the black arrow in the seismic section mark the location of the continent-ocean boundary (COB) proposed by Gaina et al. (2007). Other abbreviations: EANT – East Antarctica, MCA – MacRobertson Coastal Anomaly. (For interpretation of the references to colour in this figure legend, the reader is referred to the web version of this article.)

In contrast to the SKP crust of the northern part of the profile, the crust below the PET is only composed of two different velocity layers. The uppermost crustal layer (P_{c2}) has an average thickness of 2 km in the central part of the PET and thickens significantly towards the shelf (6 km) and the SKP (2.6 km). The upper crust in the central part of the PET (Fig. 4; OBS 203) has been modelled with velocities of $5.7\text{--}6.1 \pm 0.1$ km/s that decrease both northwards towards the SKP ($4.7\text{--}5.1$ km/s) and southwards towards the shelf ($4.8\text{--}5.4 \pm 0.1$ km/s) (Fig. 11). The base of the uppermost crustal layer is constrained by some reflections ($P_{c2}P$, Figs. 3–4). The average P-wave velocity in the lowermost crustal layer is also higher in the central part of the PET ($6.8\text{--}7.3 \pm 0.2$ km/s) compared to the sections towards the SKP ($6.4\text{--}6.8 \pm 0.2$ km/s) or the continental shelf ($6.7\text{--}6.9 \pm 0.2$ km/s). Its thickness varies between 2.3 and 5 km. The thinnest lowermost crustal layer is present where the Moho is the shallowest (Fig. 11a; ~11 km depth at km 290–312). Moho depth is well constrained by numerous reflections and increases towards the shelf (16 km depth) and towards the SKP (25 km depth). Refracted mantle phases (P_n) with a velocity of 8.0 km/s are very sparse (Fig. 10) and can only be observed at one station around magnetic chron M4n (Fig. 1b; OBS 205). 1.1.1.1.1.1.1. P-Wave velocity model resolution and uncertainties

The *rayinvr* software allows for formal error analysis and estimates of the quality of the model (Zelt and Smith, 1992). Table 1 summarizes the RMS (root mean square) misfits of different refracted and reflected phases. The assigned travel time pick uncertainties increase with the average depth of the picked phase and range between 0.025 and 0.1 s. Our P-wave velocity model has an RMS misfit of 0.066 s, which means that our model is well constrained. The χ^2 value, an indication of the misfit between modelled and picked phases, is 0.834, and slightly below the optimal value of 1.

The pick uncertainties of all modelled layers are also graphically indicated by the lengths of the pick symbols in Fig. 9. The ray coverage (Fig. 10) shows which velocity layers are well constrained by refracted arrivals and which layer boundaries are constrained by reflected phases.

In Fig. 11b the final velocity depth model is overlain by the raytraced phases to show the overall ray coverage for the model.

To estimate the velocity uncertainties of the model, we perturbed the depths of the layer boundaries and velocities until calculated travel times no longer fell within the assigned travel time error bars. This procedure resulted in seismic velocity errors for the sediments and upper crustal layers of ± 0.1 km/s and ± 0.2 km/s for the lower crust. The depth errors for the sedimentary layer are ± 0.5 km, and ± 1 km for the base of the crustal layers.

2. Gravity data and modelling

We acquired shipboard gravity data and helicopter magnetic data along and parallel to the deep seismic sounding line. RV Polarstern's Bodenseewerke gravity meter (KSS-31) recorded gravity data continuously during the entire experiment. For the land reference gravity measurements (IGNS ties), a LaCoste Romberg gravity meter (G-877) was used in Punta Arenas (Chile), at Davis Station (Prydz Bay, Antarctica), Port-aux-Français and Drygalsky Station (Kerguelen Islands), and in Cape Town (South Africa) (Hubberten, 2008). The gravity data were standard processed by applying Eötvös and latitudinal corrections and reducing the data to the gravity reference field according to the IGNS reference station readings at Punta Arenas.

A 2D gravity model was constructed to test our velocity-depth model. We used the module *GM-SYS Profile Modelling* within *Seequent's Geosoft Oasis montaj*. Here, the gravity model response is calculated using formulas introduced by Talwani et al. (1959) and Talwani and Heirtzler (1964). The model boundaries are extended 30,000 km beyond the model space to avoid edge effects.

First, we implemented the layer boundaries from the velocity model (Fig. 11) as topographic boundary conditions, and assigned layer densities according to an empirical velocity-density relationship of Ludwig et al. (1970). These initial densities are summarized in Table 2. The observed/modelled data as well as the final gravity model are shown in

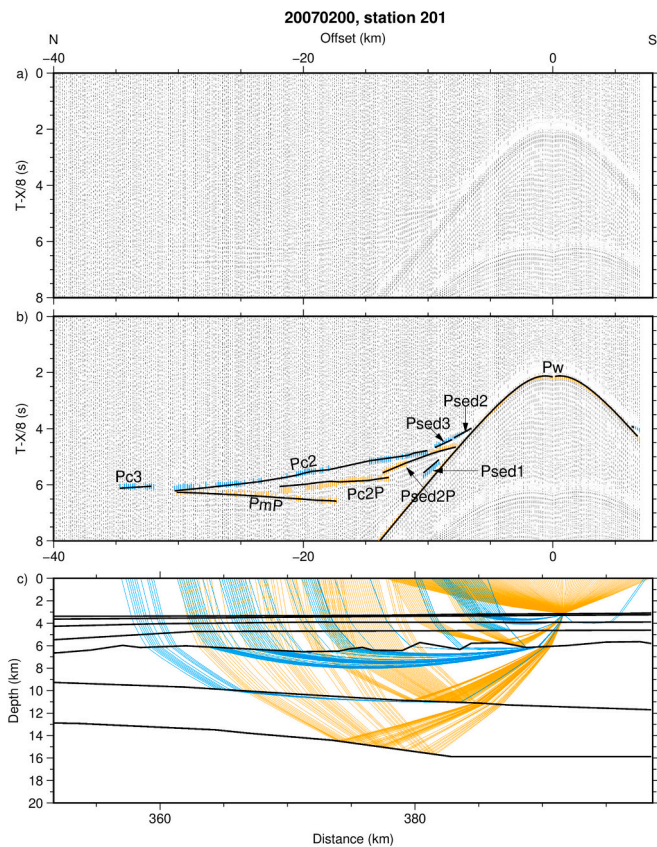


Fig. 3. Seismic record section of OBS 201 located within the continent-ocean transition of the East Antarctic margin. For its exact position see Fig. 1b. Upper panel: filtered seismic data, the data are reduced with a velocity of 8 km/s; middle: the identified phases are labelled, lower: the final velocity model overlain by the ray coverage for this OBS station.

Fig. 12. Where necessary, vertical blocks with differing densities were introduced according to changes in observed velocities of the respective layer (Table 2).

2.1. Magnetic data

In addition to Polarstern's shipboard fluxgate sensors, aeromagnetic data were collected with a Scintrex Caesium vapor magnetometer to allow for a sound identification of magnetic seafloor spreading anomalies, if present. The sensor was towed 30 m below the helicopter and recorded 4–8 profiles parallel to seismic line AWI-20070200, delivering a swath of up to 30 km width centered on the seismic profile (Fig. 1b). Standard corrections and processing steps were applied to the magnetic data (for details see Jokat et al., 2021). No diurnal corrections were conducted as no base station data were available due to the malfunction of a land-based reference station. However, the processed 3-component shipboard magnetic data as well as data from a permanently installed fluxgate magnetometer at Davis Station (Fig. 1a) indicated a relatively quiet geomagnetic field during the helicopter surveys (Hubberten, 2008). Jokat et al. (2021) modelled and interpreted magnetic reversal isochrons along the central profile of the swath. Their identifications (Fig. 1b) are used for our interpretation.

2.1.1. Results

Our deep seismic profile was acquired across the PET along 83°E (Fig. 1). It crosses the point of minimum separation between the SKP and East Antarctic continental margin. The rifted/stretched Antarctic continental margin in the research area could not be surveyed all the way to the coast, because of thick sea ice. A gravity anomaly gradient (Fig. 12)

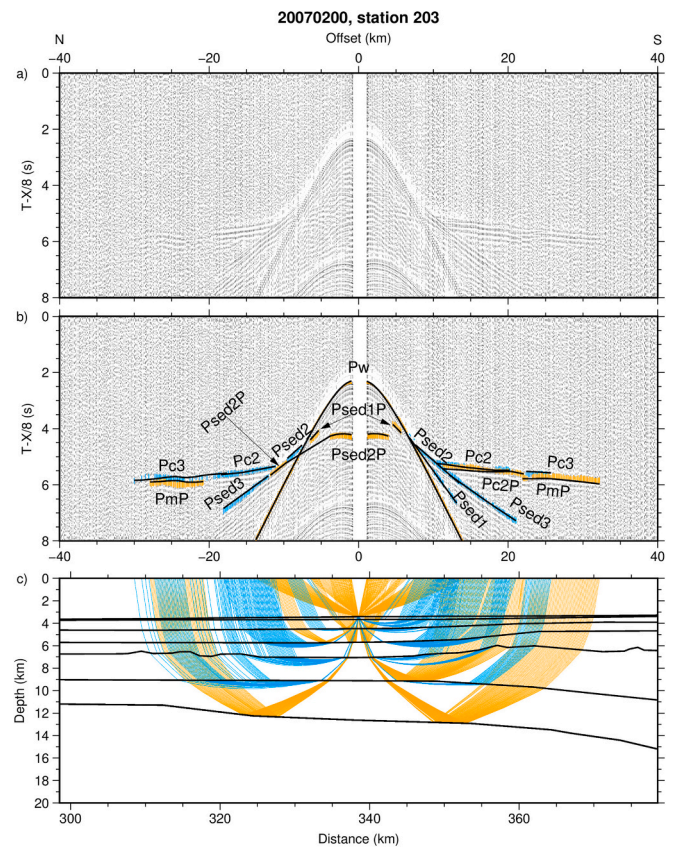


Fig. 4. Seismic record section of OBS 203 located within the oceanic part of the profile. For its exact position see Fig. 1b. Upper panel: filtered seismic data, the data are reduced with a velocity of 8 km/s; middle: the identified phases are labelled, lower: the final velocity model overlain by the ray coverage for this OBS station.

shows, however, that the crustal thickness at the southern end of the seismic line, where no seismic constraints exist, is thicker than shown in the velocity-depth model (Fig. 11a). The gradient is better explained by a dipping Moho that reaches a depth of 22 km by km 400, indicating that the southern end of the line lies within the region of crustal thinning that formed during the rifting of the Indian and Antarctic plates. At km 365, the COB is identified by combining the seismic refraction velocities and the onset of magnetic spreading anomalies interpreted from the helicopter magnetic survey (Figs. 1b, 11a; Jokat et al., 2021). The crust at the COB is about 7 km thick and shows strong variations in seismic velocities. Upper crustal velocities increase oceanwards from 5.0 ± 0.1 km/s to 5.2 ± 0.1 km/s to $5.8\text{--}6.0 \pm 0.1$ km/s, and the lower crustal velocities from 6.8 ± 0.2 km/s to as much as 7.2 ± 0.2 km/s. The oceanic crust thins northwards to 4 km over the next 75 km (Fig. 11a, km 290). Starting at km 290, the crust starts to thicken continuously northward over magnetic chron M4n (Fig. 11a; Jokat et al., 2021; 130 Ma). Within this pattern, the upper oceanic crustal layers retain an almost constant thickness, whilst it is the lower crustal layer that thickens northwards. Below ODP Leg 119 Site 738 (Fig. 11; close to OBS Station 212, red dot) the crust is almost 21 km thick. At the northern termination of the seismic profile, the Moho reaches a depth of 25 km. Here, the lower crust reaches its maximum thickness of 17 km along our line, with seismic velocities ranging from 6.8 ± 0.2 km/s to slightly more than 7.0 ± 0.2 km/s. The crustal thickening north of km 290 indicates a quickly increasing melt supply from the Kerguelen plume.

2.1.1.1. Gravity. Along the profile, the observed free air anomaly data varies over a wide range, between 32 mGal and -51 mGal. The strength of these variations can be divided into three different segments: (1) the

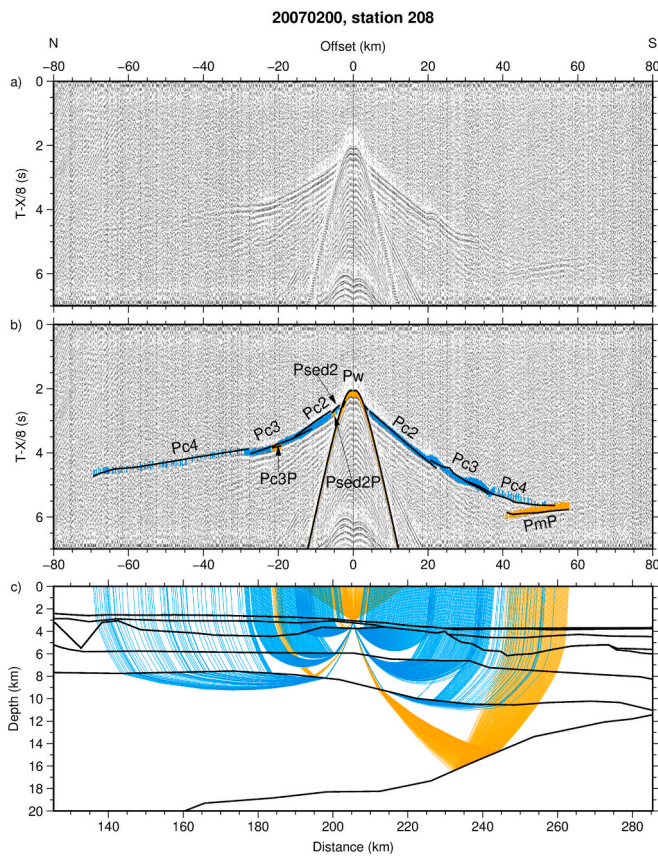


Fig. 5. Seismic record section of OBS 208 located already on the SKP. For its exact position see Fig. 1b. Upper panel: filtered seismic data, the data are reduced with a velocity of 8 km/s; middle: the identified phases are labelled, lower: the final velocity model overlain by the ray coverage for this OBS station.

SKP from km 0 to 180, which sees only small gravity variations from 13 mGal to 32 mGal; (2) the transition between the northern PET and the SKP from km 180 to 270 km, with variations from -12 to 28 mGal; and (3) the PET with its transition to the East Antarctic shelf from km 270 to 400, with large gravity variations from 32 to -51 mGal (Fig. 11a). To fit the modelled and observed gravity, the depth boundaries of the velocity-depth model (Fig. 12) had to be slightly modified. First, to account for the negative trend of modelled gravity in the northern part of the profile (km 0–120), an additional layer with a density of 3.15 g/cm^3 was introduced into the high velocity lower crustal layer (Fig. 12). For the lower crust no velocity information from seismic diving waves is available (Fig. 10, 11b). Thus, its velocity was estimated from the reflected wave (PmP) at the crust-mantle boundary (Moho). Therefore, higher lower crustal seismic velocities beneath the SKP than modelled in Fig. 11a might be present. Second, at the southern end of the profile (Fig. 11a, km 380–400), where the base of the crust in the seismic velocity model lies flat at a depth of 16 km but is not constrained by any ray coverage (Fig. 11b), the observed gravity shows a steep gradient indicating that the Moho continues to deepen southwards (Fig. 12). To fit the observed gravity, we adjusted the gravity model's Moho boundary so that it deepens to 22 km at the model's southern limit. This fits very well with results of Leitchenkov et al. (2019) along our deep seismic line, but their model terminates closer to the East Antarctic coast line approximately 50 km more to the south. They modelled a maximum Moho depth of 25–28 km beneath the continental shelf.

Overall, there is a good fit between modelled and observed gravity data, suggesting a well-constrained crustal thickness and density distribution. Larger deviations occur only near small-scale (3D?) structures. In summary, gravity residuals between the modelled and observed

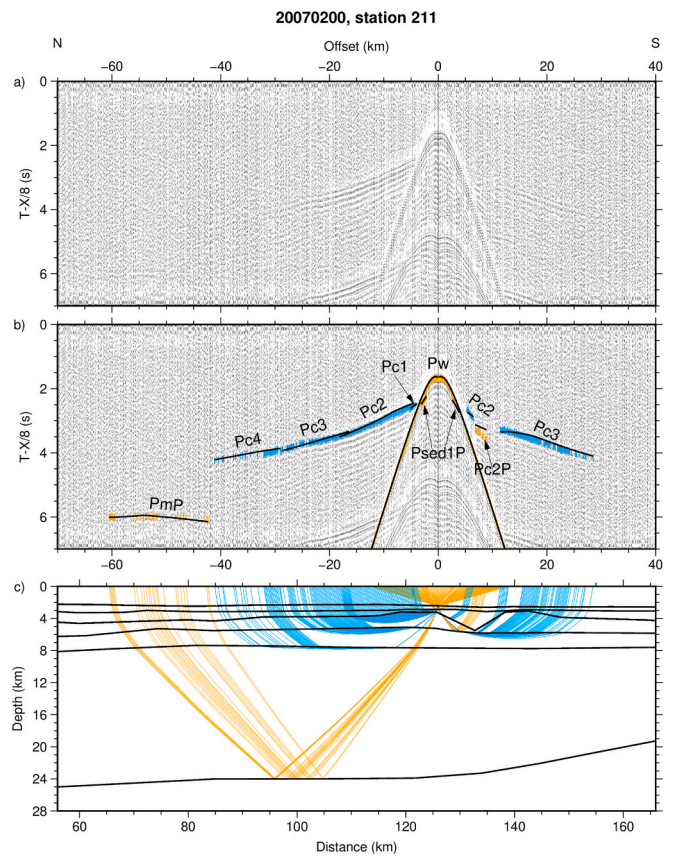


Fig. 6. Seismic record section of OBS 211 located already on the thick crust of the SKP. A PmP reflection constrains the crustal thickness of the SKP below the OBS. For its exact position see Fig. 1b. Upper panel: filtered seismic data, the data are reduced with a velocity of 8 km/s; middle: the identified phases are labelled, lower: the final velocity model overlain by the ray coverage for this OBS station.

gravity lie within 2 mGal along most of the profile, reaching a maximum of 5 mGal at around km 95. An error range of ± 5 mGal is shown as grey lines in Fig. 12. This range is acceptable for 2D gravity modelling.

2.1.1.1.1. Interpretation. Age control for the oceanic crust along this line is provided by interpreting magnetic spreading anomalies (Jokat et al., 2021). These data also provide important constraints for an estimate of the magmatic eruption volume along the 2D seismic profile. For the oceanic crust directly north of the COB (Fig. 11a; km 365–290), our velocity-depth model infers a decreasing magmatic activity. While the 133.5 Ma old oceanic crust (M9r) close to the COB is around 7 km thick, it thins to only 4 km (Fig. 11a; km 290), where magnetic chron M4n (time interval 3.5 Myrs) is observed. Interestingly we observe a small lower crustal HVL between km 300 to 340 underlying the thin oceanic crust. It has a maximum thickness of 2 km at km 310, which represents $\sim 50\%$ of the entire oceanic crust. From here the HVL quickly thins towards to north and south. Such a high velocity layer with a similar thickness, but with a larger extend, is also observed along our deep seismic line more towards the west (Altenbernd-Lang et al., 2022). We interpret this high velocity lower crust to be an indication for the first arrival of a minor amount of melt from Kerguelen plume. During the 3.5 Myr-interval of the formation of thin oceanic crust, the half spreading rate varies between 20 and 38 km/Myr (Jokat et al., 2021). North of magnetic chron M4n, the next solid age control comes from basalts drilled in Hole C at ODP Leg 119 Site 738 on the SKP, which provided an $^{40}\text{Ar}/^{39}\text{Ar}$ age of 113 ± 3.5 Ma (Jiang et al., 2021). Site 738 coincides approximately with OBS Station 212 (Fig. 11a, km 100). The steady thickening of the lower igneous crust between Site 738 and M4n suggests that the mid-ocean ridge in PET came into receipt of a quickly

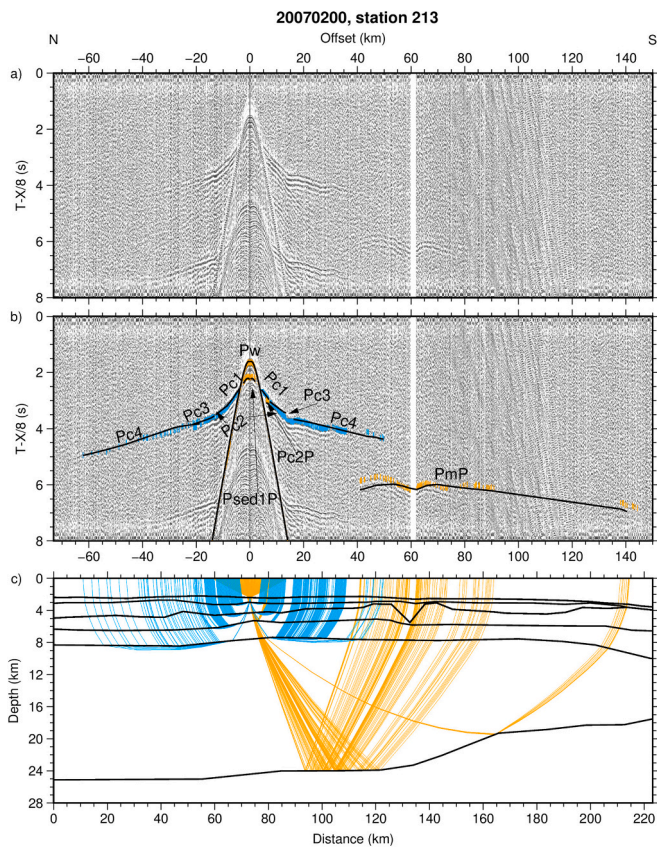


Fig. 7. Seismic record section of OBS 213 located already on the thick crust of the SKP. A strong PmP reflection constrains the crustal thickness of the SKP below the OBS. For its exact position see Fig. 1b. Upper panel: filtered seismic data, the data are reduced with a velocity of 8 km/s; middle: the identified phases are labelled, lower: the final velocity model overlain by the ray coverage for this OBS station.

increasing volume of melt from the Kerguelen plume approximately over at least a 17 Myr-long time interval 130–113 Ma. At km 120 (Fig. 11a) the crustal thickness reaches its maximum of 22–23 km and remains more or less constant until the northern end of the profile. For the northern end of our profile, we have no solid age control due to the lack of dateable spreading anomalies and drilled rock samples. The nearest drill location, ODP Leg 183 Site 1136, is located approximately 357 km further to the north. For times younger than 120 Ma, there is no sound knowledge on the spreading rates in the Enderby Basin and PET, because no continuous spreading anomalies can be identified during the Cretaceous Normal Superchron.

2.1.1.1.1. Discussion

Three deep seismic lines, one off Sri Lanka and two in the Enderby Basin, all with dense coincident magnetic surveys (Jokat et al., 2021), have been acquired to test the two-phase geodynamic model for the initial drift of the Indian plate (Gaina et al., 2007). Together, they provided new constraints for the breakup of Antarctica and India, which will be discussed here with particular focus on the analysis of a seismic refraction line across the PET and SKP, which clarifies the crustal composition of the southernmost SKP and the location of the COB off East Antarctica. 2.1.1.1.1.1. Crustal composition of the Southernmost Kerguelen Plateau

The crustal thickness along profile AWI-20070200 and its velocity-depth distribution are critical parameters for assessment of the crustal composition of the southernmost SKP, which is considered to represent the conjugate continental margin to East Antarctica. The assessment can be undertaken by comparing the plateau's velocity-depth distribution with those of better-known continental, oceanic and magmatic

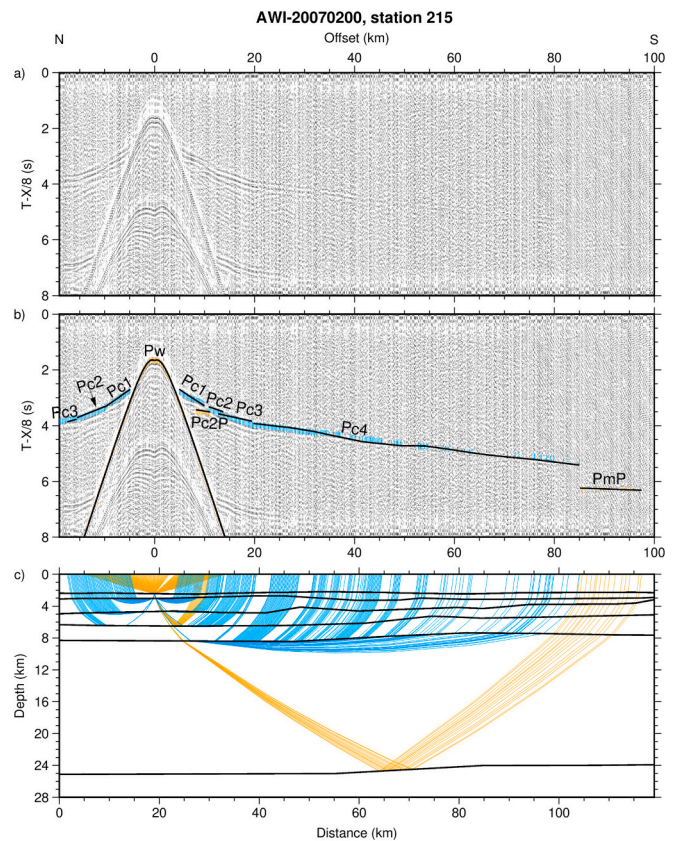


Fig. 8. Seismic record section of OBS 215 located at the northern end of the line. For its exact position see Fig. 1b. Upper panel: filtered seismic data, the data are reduced with a velocity of 8 km/s; middle: the identified phases are labelled, lower: the final velocity model overlain by the ray coverage for this OBS station.

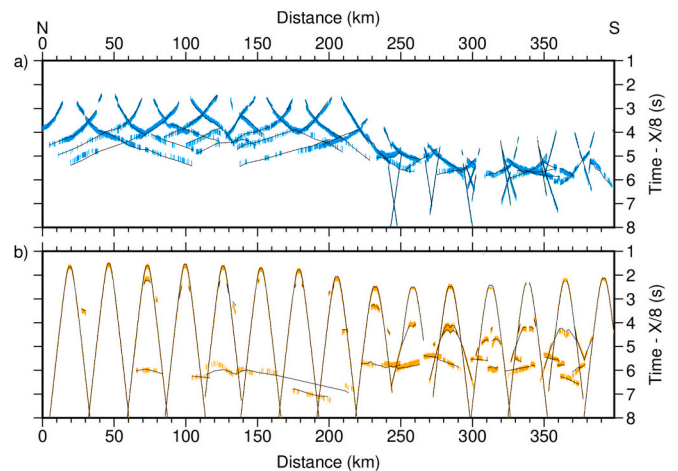


Fig. 9. The picked phases and the ray traced travel times are shown for each OBS along the line. The data are reduced with a velocity of 8 km/s. The upper panel (blue) shows the refracted phases, while the lower panel (orange) displays the reflected arrivals. The error bars vary in length according to the picking error of the value. (For interpretation of the references to colour in this figure legend, the reader is referred to the web version of this article.)

submarine plateaux/features from other settings worldwide (Fig. 13).

Our comparison of the thin crust in PET with results of global studies (Fig. 13a) shows that this part of our seismic line fits very well with the velocity-depth distribution of global oceanic crust (White et al., 1992).

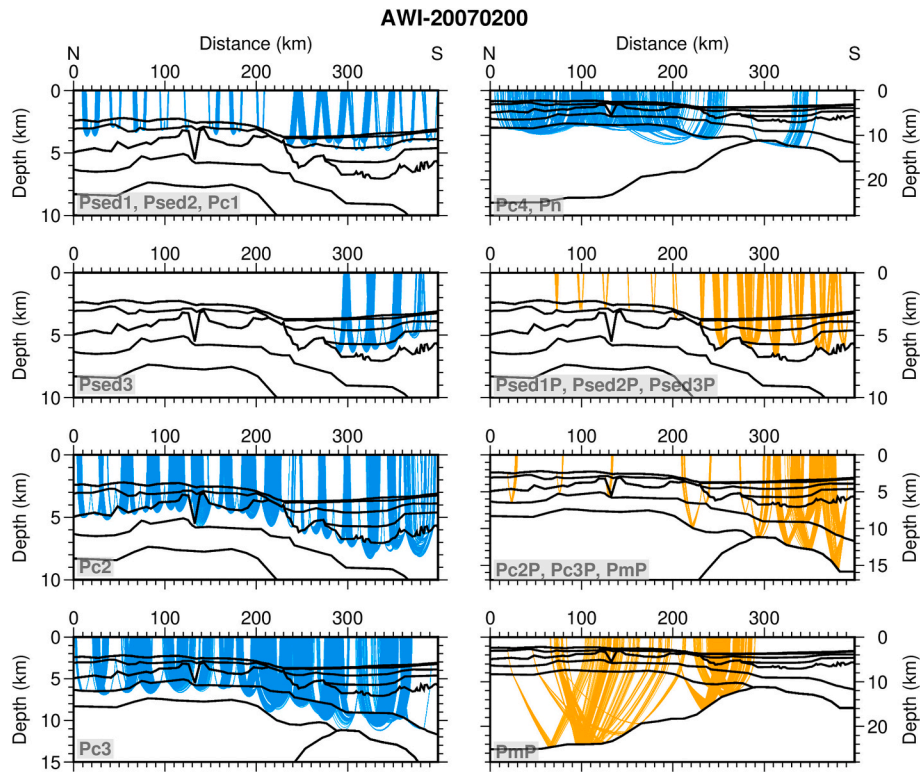


Fig. 10. Ray coverage for refracted (blue) and reflected (orange) phases along the final velocity model. (For interpretation of the references to colour in this figure legend, the reader is referred to the web version of this article.)

Fig. 13b extends the comparison to include a previous MD66/KeOBS seismic refraction line, Line 7, imaged the crust southwest of Elan Bank (Fig. 1a). This shows that the upper crust of Line 7 also fits very well into the global range for oceanic crust, whilst the lower crust is over-thickened, indicating the increasing magma supply of the Kerguelen plume (Charvis and Operto, 1999). In Fig. 13c, velocity-depth functions close to two drill sites on the SKP (blue, close to ODP Leg 119 Site 738, and red, approximately 100 km further south over the region of crustal thickening) are compared to those of extended continental crust derived from global studies (Christensen and Mooney, 1995). There is no strong likeness, indicating that the southernmost SKP is unlikely to be underlain by extended continental crust.

Two deep seismic lines were acquired in 1991 over the SKP, approximately 500 km north of the termination of our profile (Operto and Charvis, 1995, 1996; lines 4 and 5). Moho depths between 23 and 26 km were detected along them. Their lower crustal velocities constantly increase from 6.6 km/s at 9 km depth to 6.9 km/s at 19 km depth. There is a very close resemblance to the functions over our seismic line (Fig. 13d), which show a steadily increasing lower crustal velocity down to the crust-mantle boundary. What is more, these velocity-depth functions are closely reminiscent of those at other large submarine magmatic plateaux/ridges (Fig. 13e) (Grevemeyer et al., 2001; Fromm et al., 2015; Hochmuth et al., 2019).

Fig. 13f provides a comparison with heavily intruded continental crust of the Hatton Bank (White et al., 2008) and extended continental crust of the Mendeleev Ridge (Kashubin et al., 2018). The two functions representing oceanic crust (Fig. 13f, km 200, Hatton oceanic crust) show a similar Moho depth but have a different velocity gradient for oceanic layer 3.

With the last panels, we test the hypotheses that the SKP crust along lines 4 and 5 (Fig. 1a, Operto and Charvis, 1996) consist of a fragment of possibly continental lower crust overlain by a basaltic upper crust. If such a fragment exists, Operto and Charvis (1996) suggested that the crustal thickness vary between 15 and 20 km compared with a total

thickness of 22–23 km along these lines.

In Fig. 13g, results from several experiments across the Iceland-Faroe Ridge (IFR) and north of the Faroe islands are shown (Bohnhoff and Makris, 2004; White et al., 2008). This area is considered to be affected by the eruption of the Iceland plume producing also thick oceanic crust. The two velocity-depth functions along the Faroe profile indicate the difference between the continental and oceanic part of the profile. While our data at km 200, where the Kerguelen Plateau first becomes topographically visible, is very similar to the thick oceanic crust north of the Faroe Islands, our northernmost function is quite different from the velocity distribution of the Faroe continental margin. This is also the case when comparing it with data across the southeastern part of the IFR (Bohnhoff and Makris, 2004), located still within transitional/extended continental crust.

In the last panel (Fig. 13h), we show three examples of continental large igneous provinces (LIP) (Faroe, continental - White et al., 2008, Emeishan LIP - Xu et al., 2015, Deccan LIP - Tewari and Kumar, 2003), where the continental crust is assumed to be heavily intruded by plume activities. All velocity-depth functions of the SKP have a distinct different velocity depth distribution compared with those of the Kerguelen Plateau. Based on these observations, we conclude that there is no compelling evidence to interpret the southernmost tip of the SKP as being extended continental crust.

In contrast to our conclusion, several studies (Operto and Charvis, 1995, 1996; Borissova et al., 2003) have interpreted the presence of extended continental crust below parts of the Southern Kerguelen Plateau. These interpretations depend on the assumption of the existence of a reflective low-velocity layer with a mean seismic velocity of 6.7 km/s (Figs. 1, 11d) immediately above the Moho along line 4 and across Elan Bank. This low velocity layer was neither observed directly by a gap in the travel time curve nor by diving waves, but instead suggested from the time delay between two parallel seismic phases observed at larger offsets. This phase was only observed along line 4, which Operto and Charvis (1996) attributed to azimuthal anisotropy

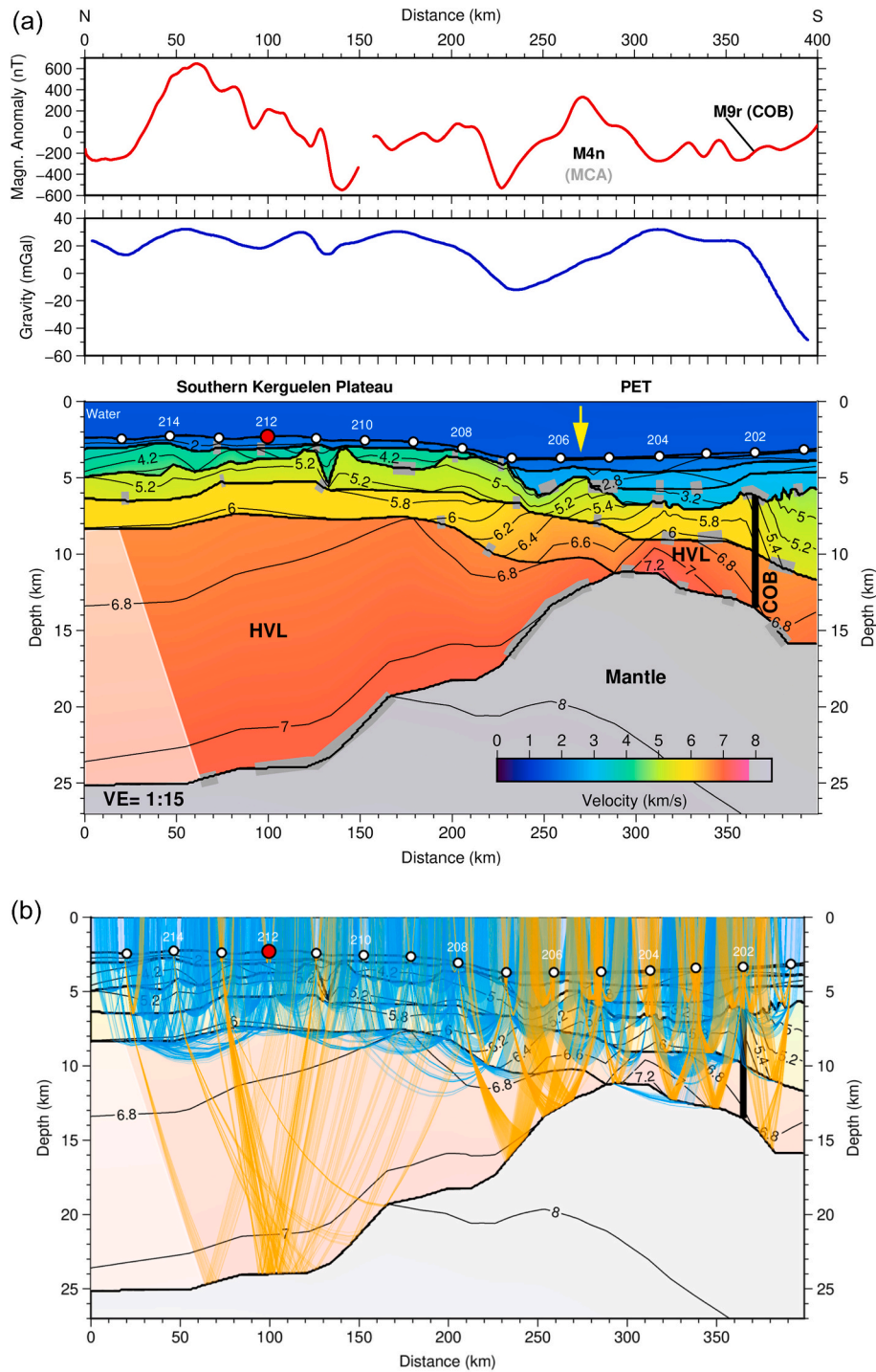


Fig. 11. a Final velocity-depth model with labelled locations of the OBS. The position of the COB is according to [Jokat et al. \(2021\)](#). The velocity contour lines are labelled in km/s. The location of OBS-212 is marked with a red dot to indicate that this instrument is closest to ODP Site 738 ([Fig. 1b](#)). The upper panel shows the magnetic data along the line with identified magnetic chrons, the middle one displays the gravity along the line. The areas constrained by reflections are marked by thick grey lines. MCA (darkgrey) marks the magnetic anomaly, which has been interpreted as continent-ocean boundary (e.g. [Gaina et al., 2007](#)). The yellow arrow indicates the COB position in the velocity model. The transparent area at the northern end of the line marks the area where no ray coverage constrains the crustal composition. Abbreviations: HVL - High Velocity Layer; VE: Vertical Exaggeration. (For interpretation of the references to colour in this figure legend, the reader is referred to the web version of this article.)

Fig. 11 b Final velocity model (transparent) overlain by all raytraced phases. The ray paths are identical with those shown in [Fig. 10](#). Reflections are plotted in orange, refracted arrivals in blue. The seismic velocities are given in km/s. Other features are identical with those of [Fig. 11a](#). (For interpretation of the references to colour in this figure legend, the reader is referred to the web version of this article.)

Table 1
Number of picks, Trms, and chi-squared.

Phase	No. of picks	Trms (s)	chi-squared
P _w	2347	0.046	0.808
P _{sed1}	295	0.062	1.380
P _{sed1} P	107	0.063	1.135
P _{sed2} , P _{c1}	380	0.050	0.776
P _{sed2} P, P _{c1} P	317	0.050	0.496
P _{sed3}	284	0.067	0.910
P _{sed3} P	248	0.076	0.836
P _{c2}	1458	0.074	0.969
P _{c2} P	192	0.094	1.521
P _{c3}	1711	0.065	0.645
P _m P, P _{c3} P	251	0.063	0.490
P _{c4}	1042	0.080	0.761
P _m P	443	0.098	1.130
P _n	32	0.063	0.502
Total	9107	0.066	0.834

In order to keep the model simple and with as few layers as possible, some layers were used to model both sediments in the southern part of the model and, for example, basaltic layers in the northern part of the model (e.g. P_{sed2}P, P_{c1}P). Since we could not pick first arrivals of the top sediment layer south of the SKP, P_{sed0} and P_{sed0}P are not included in the table.

Table 2
P-wave velocities and associated densities for individual layers and blocks used for the gravity modelling.

Layer	Type	P-wave velocity [km/s]	Density - initial model [g/cm ³]	Density - final model [g/cm ³]
Water	Water	1.5	1.03	1.03
Sediment 1 (Shelf)	Sediment	1.9	1.90	1.90
Sediment 2 (All)	Sediment	2.0	2.07	2.07
Sediment 3 (Shelf)	Sediment	2.8–3.0	2.25	2.28
Sediment 4 (Shelf)	Sediment	3.2	2.30	2.30
Sediment 5 (Plateau)	Sediment	4.2	2.35	2.35
Upper Crust	Cont.	5.0–6.0	2.65	2.58–2.86
	Oc.	5.0–6.0	2.65	2.60–2.69
Lower Crust	Cont.	5.8–7.2	2.72	2.75–3.03
	Oc.	5.8–7.2	2.72	2.67–2.81
HVL (SKP)	Oc.	6.8–7.0	3.1	3.00–3.15
Mantle (Shelf+PET)	Mantle	8.0	3.28	3.31
Mantle (SKP)	Mantle	8.0	3.28	3.27

imparted during crustal extension. Our seismic line is not suitably oriented to test this possibility. In our opinion, however, the structure of the low-velocity layer (alternating thin high/low velocity layers) is highly speculative and may have been introduced so that the velocity-depth functions more closely resemble those from typical continental crust.

Geochemical analyses of basalt samples drilled during ODP legs (Royer and Coffin, 1992; Frey et al., 2002) and results of a deep seismic sounding data (Borissova et al., 2003) have also led to proposals that the Elan Bank and SKP may be underlain by continental crust (e.g. Weis et al., 2001; Nicolaysen et al., 2001). Fig. 13 shows that these hypotheses are in conflict with our seismic analysis model. Weis et al. (2001) inferred from geochemical characteristics that the erupted basalts were contaminated by components of continental affinity. The problem in interpreting such results is that there is no unequivocal geochemical tracer to constrain the depth of the continental signature's source "... that allow distinction between a shallow source of a continental signature in oceanic basalts versus deep recycled continental material within

a mantle plume" (Class and le Roex, 2011). In attempting to distinguish between these possibilities, Weis et al. (2001) referred to the recovery of garnet-biotite gneiss clasts from a fluvial conglomerate layer cored at Site 1137. They noted that the clast lithologies were similar to rocks known from the Indian continent (Nicolaysen et al., 2001), but that their size and angularity suggested they had not been transported over a long distance before being deposited on Elan Bank. This led to the conclusion that the source of widespread continental contamination in the Kerguelen basalts is the presence of continental basement beneath Elan Bank, rather than recycling via the deep mantle.

3. Position of the COB in the Enderby Basin (50° - 90°E)

The two deep seismic lines (Altenbernd-Lang et al., 2022; this study) provide sound constraints on the position of the onset of oceanic crust at the COB in the Enderby Basin. In previous studies, it was difficult to identify this structural boundary, because seafloor spreading anomalies were not originally identified south of the MacRobertson Land/Enderby Basin Anomaly, which now has been identified as magnetic seafloor spreading anomaly M4n. The two datasets of densely spaced helicopter magnetic records (Jokat et al., 2021; Altenbernd-Lang et al., 2022; this study) showed that weak short-wavelength seafloor spreading anomalies, interpretable in the sequence back to chron M9r, do exist south of chron M4n. Thus, they proposed the COB to be located up to 160 km closer to the Antarctic continental margin. This made it necessary to refine the geodynamic model for the early drift of the Indian plate (Jokat et al., 2021).

To extrapolate our results, we use existing seismic reflection data from the SDLS data base to determine the location of the COB and the onset of the Kerguelen plume extra melt supply along the entire Antarctic continental margin between 50°E and 90°E. The main observation we utilize is the dip of the top of acoustic basement in the seismic reflection data, which becomes horizontal over the first oceanic crust. Such an approach, supplementarily constrained by magnetic spreading anomalies, has been successfully applied in several studies in different areas (e.g. Voss et al., 2009; Müller et al., 2016; Jokat et al., 2021; Altenbernd-Lang et al., 2022), and is ideal for use with the relatively dense seismic reflection data network, including many Russian seismic reflection profiles (Figs. 14 and 15), in the PET and Enderby Basin (Fig. 16). Investigating the entire continental margin from 55°E to 90°E made it necessary to slightly refine the COB location of Altenbernd-Lang et al. (2022) (Fig. 16; dashed black line vs green dots-new estimate; see also supplementary material). Our seismically interpreted COB is compared with a gravity study for the Enderby Basin and the PET (Davis et al., 2019), showing mostly negligible disagreement. The exception is an area between 65°E to ~76°E. Here, the largest differences occurred. E.g., along a deep seismic line (Altenbernd-Lang et al., 2022) the seismically derived COB is approximately 80 km north of the gravity modelled COB (Davis et al., 2019). In the PET both COB estimates perfectly fit along our deep seismic line. Finally, it is interesting to note that, independently of our new geophysical data (Jokat et al., 2021; this study), Davis et al. (2019) located the COB significantly farther south than previous studies (Stagg et al., 2004; Gaina et al., 2007; Leitchenkov et al., 2014).

3.1. Oceanic crust thickness variations

Our deep seismic data show that, between magnetic chrons M9r and M4n, the Kerguelen plume provided only a minor amount of melt to the Enderby Basin seafloor spreading ridges. Only thin oceanic crust was produced during the first 3.5 Myrs of basin formation with a high velocity lower crust (50 % of the entire crust). Both lines show that the first massive melt supply from the Kerguelen plume erupted around magnetic chron M4n (Fig. 16a, red dots; Jokat et al., 2021; Altenbernd-Lang et al., 2022). This event during M4n resulted in the development of a step in the basement topography of the oceanic crust that can be

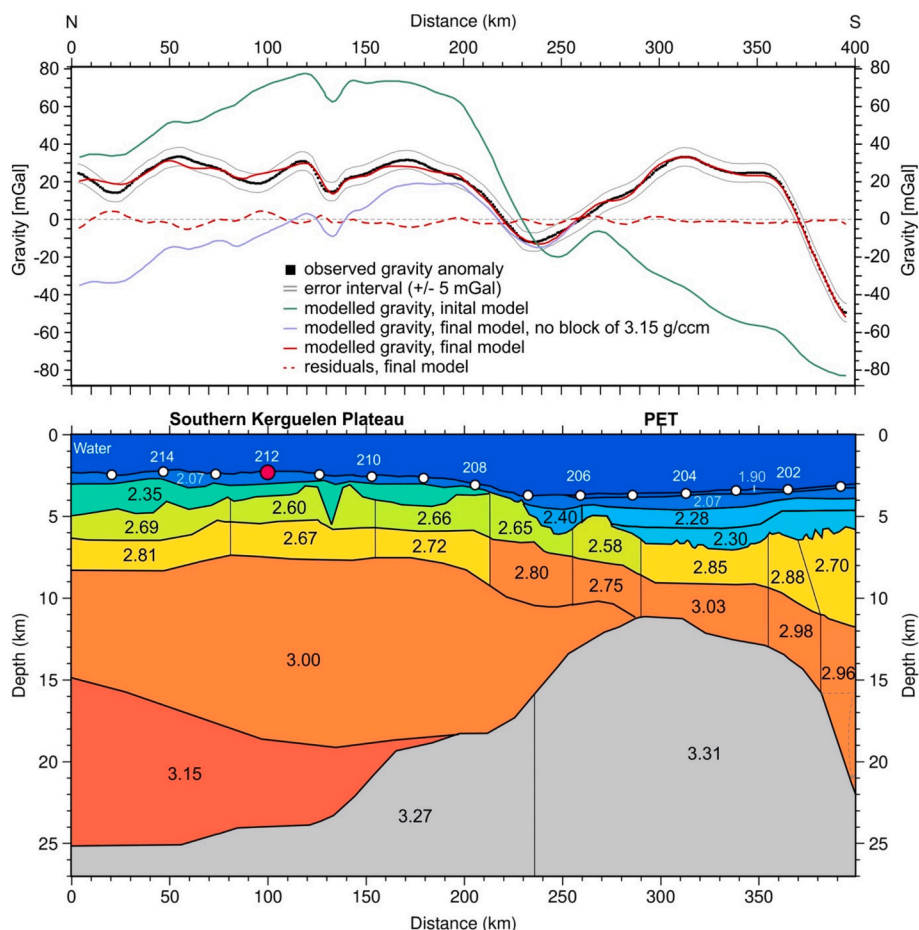


Fig. 12. Density model for the velocity-depth model (Fig. 11a). In the upper panel the original free-air gravity anomaly values (black line) as well as the results of the different modelling steps. The density values in the blocks are given in g/cm^3 . The seismic velocities were converted to densities according to Ludwig et al. (1970) and Müller et al. (2016). These initial values were slightly varied to fit the measured gravity. Landward of OBS 201, the crustal thickness is not constrained at all by any seismic phases. To fit the gravity gradient and to avoid unusual high density for the mantle, we had to increase the Moho depth to 22 km.

observed along most of the Enderby Basin's seismic reflection lines. On a few Australian seismic lines, Moho reflections also show that the oceanic crust thickens to the north of this basement step (Stagg et al., 2004). These observations led Stagg et al. (2004) to relate the step to the delivery of extra melt from the Kerguelen plume to a mid-ocean ridge in the Enderby Basin, but it was long unclear whether the step might represent that ridge's initiation at the basin's COB, or its demise as an extinct spreading axis (Stagg et al., 2004; Gaina et al., 2007; Leitchenkov et al., 2014, 2015). The new deep seismic data now clearly infer that this basement high formed within oceanic crust, whose northwards thickening is marked by the basement high and the pronounced magnetic chron M4n (Altenbernd-Lang et al., 2022). In the PET, the location of the basement step along RAE48–08 implies that excess melt arrived slightly prior to chron M4n, whereas ~400 km further west, RAE39–03 suggests its arrival just afterwards, during M3r (Figs. 14,15). At face value, this contrast suggests that plume material may have advanced westwards beneath the ridge crest, or excess melt migrated along it, at a rate of ~155 km/Myr.

Seismic wide-angle/refraction line 7 (Fig. 1; line 7; Borissova et al., 2003), which is located southwest of Elan Bank, helps to test the distribution of thickened oceanic crust in the Enderby Basin away from our two deep seismic lines. Line 7 was also acquired during the MD66/KeOBS cruise and with identical acquisition parameters as lines 4 and 5 (Fig. 1; Charvis et al., 1995). The spacing of its five OBS was around 30–40 km. The velocity distribution was interpreted as that of oceanic crust, with layer 2 velocities of 5.0 to 6.5 km/s, and layer 3 velocities of 6.7 to 7.3 km/s at the crust-mantle boundary. The velocity-depth model

shows a 14 km thick magmatic crust (oceanic layer 2 + 3) close to Elan Bank with the Moho depth at 18 km (Fig. 13b). Overlying sediments are only 30 to 300 m thick (Charvis and Operto, 1999). Along the 125 km long profile, the crustal thickness reduces southwards to 10–11 km at its southwestern termination. The Moho shallows to around 16 km. Charvis and Operto (1999) proposed that this thick oceanic crust, which is thicker than the global mean of 7 km (White et al., 1992), was created at a mid-ocean ridge that received excess melt from the Kerguelen plume. This interpretation is in general agreement with our findings based on the two newer, longer, and more detailed deep seismic lines (Jokat et al., 2021; Altenbernd-Lang et al., 2022; this study). Along the transect AWI-20120400/AWI-20070100, the crust at about 60°N is around 10 km thick, similar to that of line 7 (Fig. 1). Together, these profiles indicate that most of Enderby Basin formed under the influence of excess melt supply from the Kerguelen plume, an interpretation that is not obvious from the contrast between the deep basin and much shallower neighboring Kerguelen Plateau. We suggest this contrast might relate how the present-day Kerguelen Plateau marks an area where the main eruptions occurred.

We applied our above listed criteria to all available seismic reflection data to determine areas of oceanic crust between the continental rifted margin and the oceanic crust affected by the Kerguelen plume. Our data provide the following insights (Fig. 16):

Between 54°E and 68°E, the COB and chron M4n are well defined and the observed characteristic topographic step in the basement coincides with magnetic chron M4n.

Between 70°E and 72°E (Fig. 16b, blue box; Prydz Bay), the COB

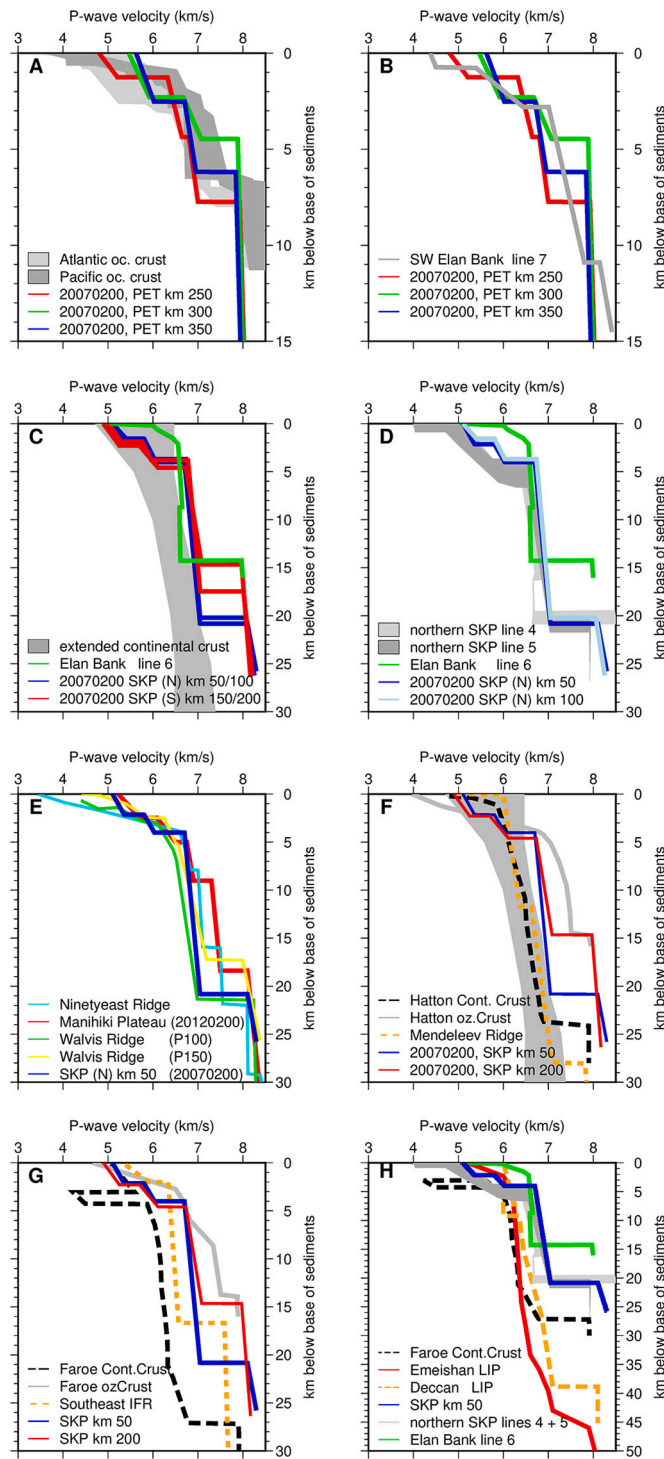


Fig. 13. Comparison of the velocity-depth (v_z) functions along line AWI-20070200. A - compare the oceanic part of the line with values for oceanic crust in the Atlantic/Pacific (White et al., 1992), B - compare the same v_z functions with overthickened crust SW of Elan Bank (Charvis and Operto, 1999), C - compare v_z functions from the SKP with a typical range of values for extended continental crust (Christensen and Mooney, 1995), D - v_z functions from the SKP are compared with MD66/KeOBS cruise data from the northern part of the SKP (see Fig. 1a for their location) (Operto and Charvis, 1995; Borissova et al., 2003); E - comparison with other large magmatic submarine plateaux/ridges (Ninetyeast Ridge - Grevenmeyer et al., 2001; Walvis Ridge - Fromm et al., 2015; Manihiki Plateau - Hochmuth et al., 2019) Christensen and Mooney, 1995), F - v_z functions, which are interpreted to represent continental or thickened oceanic crust (Hatton Bank -cont/oceanic - White et al., 2008, Mendeleev Ridge - Kashubin et al., 2018), G - v_z functions of deep seismic results acquired around the Iceland Faroe Ridge system (Faroe Ridge along strike -cont/oceanic - White et al., 2008, Iceland-Faroe Ridge across N-S direction - Bohnhoff and Makris, 2004), H - v_z functions of continental large igneous provinces (LIP) (Faroe, continental - White et al., 2008, Emeishan LIP - Xu et al., 2015, Deccan LIP - Tewari and Kumar, 2003) compared with deep seismic sounding lines on the SKP/Elan Bank.

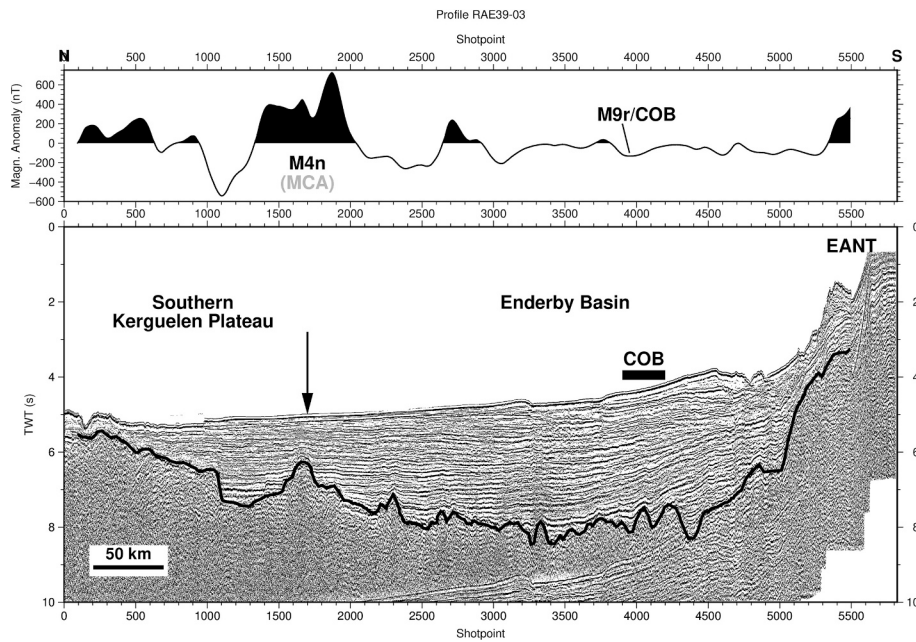


Fig. 14. Russian seismic reflection line RAE39-03 across the Enderby Basin along 77°E. The ~580 km long line shows a shallowing of the oceanic basement north of shot point 3300 south of magnetic chron M4n. We assume that this observation indicates the arrival of Kerguelen plume earlier than M4n between Prydz Bay and PET. Upper panel: magnetic data extracted from the Antarctic Digital Magnetic Anomaly Project grid (ADMMap, Golynsky et al., 2007). MCA (darkgrey) and the black arrow in the seismic section mark the location of the continent-ocean boundary proposed by Gaina et al. (2007). Abbreviations: EANT — East Antarctica, MCA — MacRobertson Coastal Anomaly.

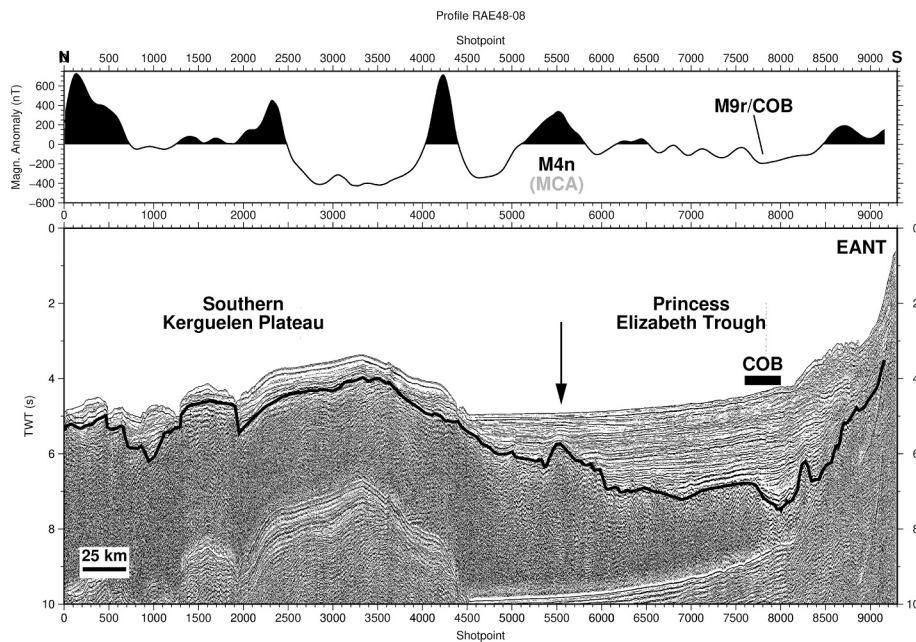


Fig. 15. Russian seismic reflection line RAE48-08 (~470 km long) across the PET along 84°E. In the eastern part of the Princess Elizabeth Trough the top of oceanic basement continues to shallow (north of shotpoint 6900) well before chron M4n. Only approximately a 40 km wide corridor of oceanic crust (shot points 6900 to 7700) has not received extra melt from the Kerguelen plume. Upper panel: magnetic data extracted from the ADMMap grid (Golynsky et al., 2007). MCA (darkgrey) and the black arrow in the seismic section mark the location of the continent-ocean boundary proposed by Gaina et al. (2007). Abbreviations: EANT — East Antarctica, MCA — MacRobertson Coastal Anomaly.

cannot be tracked/defined beneath the thick sediments of the Prydz Channel Fan, where sea floor multiples mask the top of the basement. It is likely that the basement further deepens towards the East Antarctic coast. We observe that along seismic lines GA229-30, GA229-31, RAE52-06, RAE52-07, and RAE52-11 the same pattern. The oceanic basement deepens south magnetic chron M4n, and might be a hint that

some extra melt arrived earlier in the northward prolongation of the Lambert Graben and eastward of it within the PET influencing the basement topography as observed.

At ~74°E (towards the Princess Elizabeth Trough - PET), the width of the strip of thin oceanic crust produced before a massive amount of melt was delivered by the Kerguelen plume around ~130 Ma narrows to just

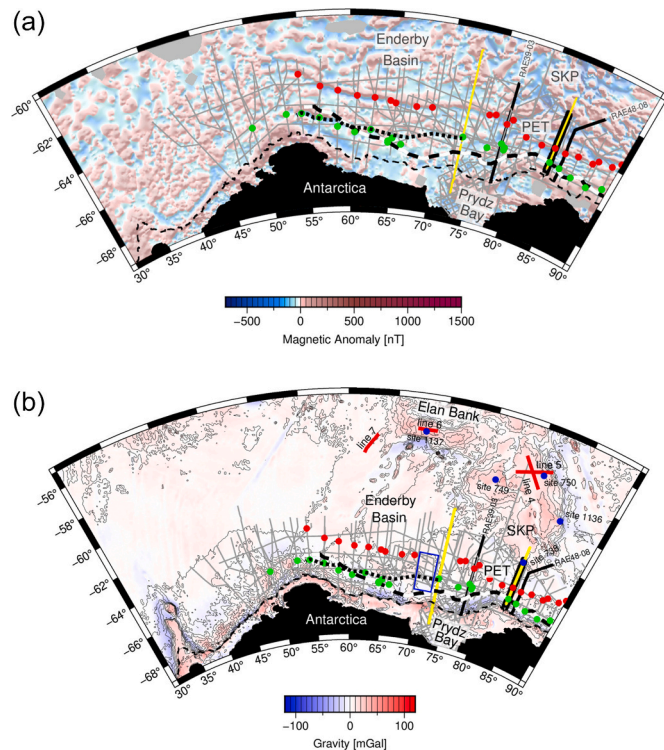


Fig. 16. **a** The map summarizes our findings. It shows the position of the COB (this study, green dots; see also supplementary material) and the location of magnetic chron M4n (this study, red dots). The ADMAP grid (Golynsky et al., 2007) is displayed as background information. Yellow lines: mark the two seismic refraction lines crossing the Enderby Basin and Princess Elizabeth Trough, black-yellow line: indicates that the position of our deep seismic refraction line is identical -except the very northern part- with the seismic refraction line RAE39-10, thick-black lines: indicate the position of three seismic reflection lines used in this study, grey transparent lines: complete seismic reflection data network, dashed line: marks the shelf break of the continental margin, white-black thick dashed line: marks the COB derived from gravity modelling (Davis et al., 2019). Abbreviations: PET - Princess Elizabeth Trough, SKP- southern Kerguelen Plateau. (For interpretation of the references to colour in this figure legend, the reader is referred to the web version of this article.)

Fig. 16 b The map has been extended to 55°S to show all existing seismic reflection and refraction lines in the research area. Comparing to Fig. 16a, the bathymetry (GEBCO Compilation Group, 2021) is plotted with a contour line spacing of 500 m underlain by the free air gravity field (Sandwell et al., 2014). Furthermore, the ODP sites (blue dots) and the MD66/KeOBS seismic refraction lines (red lines) are shown. Dashed line indicates the COB estimate of Altenbernd-Lang et al. (2022). The remaining features are identical with those of Fig. 16a. (For interpretation of the references to colour in this figure legend, the reader is referred to the web version of this article.)

40 km.

The observed, thin oceanic crust in the Enderby Basin (Altenbernd-Lang et al., 2022) and Princess Elisabeth Trough between approx. Magnetic chron M9/COB and M4n indicates that the separation of India and Antarctica was not triggered by the Kerguelen plume. Otherwise, thick oceanic crust should have been detected. This is in excellent agreement with petrological studies, which negate a plume induced separation of both plates, but favour a passive continental breakup (e.g. Coffin et al., 2002; Ingle et al., 2004; Olierook et al., 2019).

3.1.1. Conclusions

The crustal thickness and composition between the Southern

Kerguelen Plateau and the East Antarctic margin, derived from deep crustal seismic data, address the influence of the Kerguelen mantle plume during the breakup of the Indian and Antarctic plate. For the first 3.5 Myrs of the Indian plate drift, only ~4 km thick oceanic crust was formed with only a minor amount of Kerguelen melt possibly documented by high velocity lower crust just north of the COB. Off Prydz Bay and eastwards to the PET, the first excess Kerguelen plume melt arrived around 130 Ma, significant earlier than the oldest basalts drilled from the neighboring Kerguelen Plateau. The velocity-depth model for the southernmost SKP indicates that its seismic velocities are not typical of an extended volcanic continental rifted margin. Instead, the velocity distribution is similar to that of oceanic large igneous provinces like the Walvis Ridge or Ninetyeast Ridge. Thus, its evolution was similar to other large oceanic plateaux that formed in a seafloor spreading environment. We infer that the southernmost Southern Kerguelen Plateau does not consist of continental crust overlain by basalt flows.

CRediT authorship contribution statement

Wilfried Jokat: Writing – review & editing, Writing – original draft, Supervision, Resources, Project administration, Methodology, Funding acquisition, Conceptualization. **Tabea Altenbernd-Lang:** Writing – original draft, Validation, Software, Methodology, Investigation, Formal analysis. **Karsten Gohl:** Writing – original draft, Methodology, Investigation, Funding acquisition, Conceptualization. **German L. Leitchenkov:** Writing – original draft, Methodology, Investigation, Funding acquisition, Formal analysis, Data curation, Conceptualization. **Hannes Eisermann:** Writing – original draft, Methodology, Formal analysis.

Declaration of competing interest

The authors declare the following financial interests/personal relationships which may be considered as potential competing interests:

Wilfried Jokat reports financial support was provided by Alfred Wegener Institute for Polar and Marine Research, Bremerhaven. If there are other authors, they declare that they have no known competing financial interests or personal relationships that could have appeared to influence the work reported in this paper.

Acknowledgements

We thank captain and crew of RV Polarstern and RV Akademik Alexander Karpinsky for their essential support during the expeditions. We thank Polar Marine Geosurvey Expedition (PMGE) for providing the seismic reflection data. We thank Ricarda Nielsen for providing the basement picks for the seismic reflection data. Two anonymous reviewers provided helpful comments, which are greatly appreciated. The OBS and OBH were provided by the German Instrument Pool for Amphibian Seismology (DEPAS). The figures were generated with GMT software (Wessel et al., 2013). We thank the OGS Trieste (<http://sdls.ogs.trieste.it>) for providing the Antarctic Seismic Data Library System (SDLS). We thank Aspen Technology Inc. for providing seismic software licenses and support. We thank Graeme Eagles for checking the English language and for useful comments. This project was funded by institutional funds of the Alfred-Wegener-Institute Helmholtz-Zentrum für Polar- und Meeresforschung (AWI) under the POF-IV Subtopic 2.1 "Warming climates". We also acknowledge the financial support by the AWI Open Access Publication Fund.

Appendix A. Supplementary data

Supplementary data to this article can be found online at <https://doi.org/10.1016/j.tecto.2025.230804>.

Data availability

The seismic reflection data underlying this article are freely available from the SDLS data base (<https://scar.org/library-data/data/seismic-data>), while the seismic refraction and potential field data will be shared on reasonable request to the corresponding author.

References

- Altenbernd-Lang, T., Jokat, W., Leitchenkov, German L., G.L., 2022. Distribution of oceanic crust in the Enderby Basin offshore East Antarctica. *Geophys. J. Int.* 231. <https://doi.org/10.1093/gji/ggac299>, 1959–181.
- Bohnhoff, M., Makris, J., 2004. Crustal structure of the Southeastern Iceland-Faroe Ridge (IFR) from wide aperture seismic data. *J. Geodyn.* 37 (2), 233–252. <https://doi.org/10.1016/j.jog.2004.02.004>.
- Borissova, I., Coffin, M.F., Charvis, P., Operto, S., 2003. Structure and development of a microcontinent: Elan Bank in the southern Indian Ocean. *Geochem. Geophys. Geosyst.* 4 (9). <https://doi.org/10.1029/2003GC000535>.
- Cande, S.C., Kent, D.V., 1995. Revised calibration of the geomagnetic polarity time scale for the late Cretaceous and Cenozoic. *J. Geophys. Res.* 100, 6093–6095. <https://doi.org/10.1029/94JB03098>.
- Charvis, P., Operto, S., 1999. Structure of the Cretaceous Kerguelen Volcanic Province (southern Indian Ocean) from wide-angle seismic data. *J. Geodyn.* 28, 51–71. [https://doi.org/10.1016/S0264-3707\(98\)00029-5](https://doi.org/10.1016/S0264-3707(98)00029-5).
- Charvis, P., Recq, M., Operto, S., 1995. Deep structure of the northern Kerguelen-Plateau and hot spot-related activity. *J. Geophys. Res.* 122 (3), 899–924. <https://doi.org/10.1111/j.1365-246X.1995.tb06845.x>.
- Christensen, N.I., Mooney, W.D., 1995. Seismic velocity structure and composition of the continental crust: a global view. *J. Geophys. Res.* 100, 9761–9788. <https://doi.org/10.1029/95JB00259>.
- Class, C., le Roex, A., 2011. South Atlantic DUPAL anomaly — Dynamic and compositional evidence against a recent shallow origin. *Earth Planet. Sci. Lett.* 305, 92–102. <https://doi.org/10.1016/j.epsl.2011.02.036>.
- Coffin, M.F., Eldholm, O., 1994. Large igneous provinces: crustal structure, dimensions, and external consequences. *Rev. Geophys.* 32 (1), 1–36. <https://doi.org/10.1029/93RG02508>.
- Coffin, M.F., Pringle, M.S., Duncan, R.A., Gladchenko, T.P., Storey, M., Müller, R.D., Gahagan, L.A., 2002. Kerguelen hotspot magma output since 130 Ma. *J. Petrol.* 43, 1121–1137. <https://doi.org/10.1093/petrology/43.7.1121>.
- Davis, J.K., Lawver, L.A., Norton, I.O., Dalziel, I.W.D., Gahagan, L.M., 2019. The crustal structure of the Enderby Basin, East Antarctica. *Mar. Geophys. Res.* 40, 1–16. <https://doi.org/10.1007/s11001-018-9356-5>.
- Eagles, G., 2019. A little spin in the Indian Ocean plate circuit. *Tectonophysics* 754, 80–100. <https://doi.org/10.1016/j.tecto.2019.01.015>.
- Eagles, G., Eisermann, H., 2020. The Skytrain plate and tectonic evolution of Southwest Gondwana since Jurassic times. *Sci. Rep.* 10, 19994. <https://doi.org/10.1038/s41598-020-77070-6>.
- Frey, F.A., Weis, D., Borissova, A.Y., Xu, G., 2002. Involvement of continental crust in the formation of the Cretaceous Kerguelen Plateau: New perspectives from ODP Leg 202 sites. *J. Petrol.* 43, 1207–1239. <https://doi.org/10.1093/petrology/43.7.1207>.
- Frey, F.A., Coffin, M.F., Wallace, P.J., Weis, D., 2003. Leg 183 Synthesis: kerguelen plateau-broken ridge—a large igneous province. *Proc. Ocean Drill. Program Sci. Results* 183, 1–48. <https://doi.org/10.2973/odp.proc.sr.183.015.2003>.
- Fromm, T., 2016. PRay—a graphical user interface for interactive visualization and modification of rayinvr models. *J. Appl. Geophys.* 124, 1–3. <https://doi.org/10.1016/j.jappgeo.2015.11.004>.
- Fromm, T., Planert, L., Jokat, W., Ryberg, T., Behrmann, J.H., Weber, M.H., Haberland, C., 2015. South Atlantic opening: a plume-induced breakup? *Geology* 43 (10), 931–934. <https://doi.org/10.1130/G36936.1>.
- Gaina, C., Mueller, R.D., Brown, B., Ishihara, T., Ivanov, S., 2007. Breakup and early seafloor spreading between India and Antarctica. *Geophys. J. Int.* 170, 151–169. <https://doi.org/10.1111/j.1365-246X.2007.03450.x>.
- GEBCO Compilation Group, 2021. GEBCO 2021 Grid. <https://doi.org/10.5285/c6612cbe-50b3-0cff-e053-6c86abc09f8f>.
- Gibbons, A.D., van den Brackhausen, U., Bogaard, P., Hoernle, K., Werner, R., Whittaker, J.M., Müller, R.D., 2012. Constraining the Jurassic extent of Greater India: Tectonic evolution of the West Australian margin. *Geochem. Geophys. Geosyst.* 13. <https://doi.org/10.1029/2011GC003919>. Q05W13.
- Golynsky, A., Blankenship, D., Chiappini, M., Damaske, D., Ferraccioli, F., Finn, C., Golynsky, D., Goncharov, A., Ishihara, T., Ivanov, S., Jokat, W., Kim, H.R., König, M., Masolov, V., Nogi, Y., Sand, M., Stüding, M., von Frese, R., the ADMAP Working Group, 2007. New magnetic anomaly map of East Antarctica and surrounding regions. In: Cooper, A.K., Raymond, C.R., et al. (Eds.), *Proceedings of the 10th ISAES. USGS Open-File Report 2007-1047, Short Research Paper 050*. <https://doi.org/10.3133/of2007.srp050>, 4 p.
- Gradstein, F.M., Ogg, J.G., Smith, A.G., Bleeker, W., Lourens, L.J., 2004. A new Geologic time scale, with special reference to Precambrian and Neogene. *Episodes* 27 (2), 83–100. <https://doi.org/10.18814/epiiugs/2004/v27i2/002>.
- Grevenmeyer, I., Flueh, E.R., Reichert, C., Bialas, J., Klaschen, D. & Kopp, C., 2001. Crustal architecture and deep structure of the Ninetyeast Ridge hotspot trail from active-source ocean bottom seismology. *Geophys. J. Int.* 144, 414–431. <https://doi.org/10.1046/j.0956-540X.2000.01334.x>.
- Hochmuth, K., Gohl, K., Uenzelmann-Neben, G., Werner, R., 2019. Multiphase magmatic and tectonic evolution of a large igneous province - evidence from the crustal structure of the Manihiki Plateau, western Pacific. *Tectonophysics* 750, 434–457. <https://doi.org/10.1016/j.tecto.2018.11.014>.
- Hubberten, H.W., (2008). The expedition Antarktis-XXIII/9 of the research vessel “Polarstern” in 2007, *Rep. Polar Mar. Res.*, 583, 167pp. <https://epic.awi.de/id/eprint/28719>.
- Ingle, S., Scoates, J.S., Weis, D., Brüggmann, G., Kent, R.W., 2004. Origin of Cretaceous continental tholeiites in southwestern Australia and eastern India: insights from Hf and Os isotopes. *Chem. Geol.* 209, 83–106.
- Jiang, Q., Jourdan, F., Olierook, H.K.H., Merle, R.E., Whittaker, J.M., 2021. Longest continuously erupting large igneous province driven by plume-ridge interaction. *Geology* 49, 206–210. <https://doi.org/10.1130/G47850.1>.
- Jokat, W., Altenbernd, T., Eagles, G., Geissler, W.H., 2021. The early drift of the Indian plate. *Sci. Rep.* 11. <https://doi.org/10.1038/s41598-021-90172-z>.
- Jokat, W., Boebel, T., Koenig, M., Meyer, U., 2003. Timing and geometry of early Gondwana breakup. *J. Geophys. Res.* 108 (B9), 2428. <https://doi.org/10.1029/2002JB001802>.
- Jourdan, F., Fraud, G., Bertrand, H., Watkeys, M.K., 2007. From flood basalts to the inception of oceanization: example from the 40Ar/39Ar high-resolution picture of the Karoo large igneous province. *Geochem. Geophys. Geosyst.* 8, 1–20. <https://doi.org/10.1029/2006GC001392>.
- Kashubin, S., Petrov, O.V., Artemieva, I.M., Morozov, A.F., Vyatkin, D.V., Golsheva, Y. S., Kashubina, T.V., Milshtein, E.D., Rybalka, A.V., Erinchek, Y.M., Sakulina, T.S., Krupnova, N.A., Shulgin, A.A., 2018. Crustal structure of the Mendeleev rise and the Chukchi Plateau (Arctic Ocean) along the Russian wide-angle and multichannel seismic reflection experiment “Arctic-2012”. *J. Geodyn.* 119, 107–122. <https://doi.org/10.1016/j.jog.2018.03.006>.
- König, M., Jokat, W., 2006. The Mesozoic breakup of the Weddell Sea. *J. Geophys. Res.* 111, B12102. <https://doi.org/10.1029/2005JB004035>.
- Lawver, L.A., Gahagan, L.M., Dalziel, I.W.D., 1998. A tight fit – early Mesozoic Gondwana, a plate reconstruction perspective. *Memoirs Nat'l Inst. Polar Res.* 53, 214–229.
- Leitchenkov, G.L., Guseva, Y.B., Gandyukhin, V.V., Ivanov, S.V., Safonova, L.V., 2014. Structure of the Earth's Crust and Tectonic Evolution history of the Southern Indian Ocean (Antarctica). *Geotectonics*, 2014 48 (1), 5–23. <https://doi.org/10.1134/S001685211401004X>.
- Leitchenkov, G.L., Guseva, Y.B., Gandyukhin, V.V., Ivanov, S.V., 2015. *Crustal Structure, Tectonic Evolution and Seismic Stratigraphy of the Southern Indian Ocean*, VNIIOkeangeologia, 200pp. Russian, abstract and figure captions in English.
- Leitchenkov, G.L., Galushkin, Y.L., Guseva, Y.B., Gandyukhin, V.V., Dubinin, E.P., 2019. Crustal structure, tectonic subsidence, and lithospheric stretching of the Princess Elizabeth Trough Basin, East Antarctica. *Geotectonics* Vol. 53 (6), 726–737. <https://doi.org/10.31857/S0016-853X2019692-104>.
- Lisker, F., 2004. The Evolution of the Geothermal Gradient from Lambert Graben and Mahanadi Basin – A Contribution to the Indo-Antarctic Rift Debate. *Gondwana Res.* 7 (2), 363–373. [https://doi.org/10.1016/S1342-937X\(05\)70790-5](https://doi.org/10.1016/S1342-937X(05)70790-5).
- Ludwig, J., Nafe, J., Drake, C., 1970. *Seismic refraction*. In: *The Sea*. Maxwell, A.E., Wiley-Interscience, pp. 53–84.
- Müller, C.O., Jokat, W., 2019. The initial Gondwana breakup: a synthesis based on new potential field data of the Africa-Antarctica Corridor. *Tectonophysics* 750, 8. <https://doi.org/10.1016/j.tecto.2018.11.008>, 301–322004.
- Müller, C.O., Jokat, W., Schreckenberger, B., 2016. The crustal structure of Beira High, Central Mozambique - combined investigation of wide-angle seismic and potential field data. *Tectonophysics* 683, 233–254. <https://doi.org/10.1016/j.tecto.2016.06.028>.
- Nicolaysen, K., Bowring, S., Frey, F., Weis, D., Ingle, S., Pringle, M.S., Coffin, M.F., 2001. Provenance of Proterozoic garnet-biotite gneiss recovered from Elan Bank. *Kerguelen Plateau, southern Indian Ocean, Geology* 29, 235–238. [https://doi.org/10.1130/0091-7613\(2001\)029<0235:POPGBG>2.0.CO;2](https://doi.org/10.1130/0091-7613(2001)029<0235:POPGBG>2.0.CO;2).
- Nogi, Y., Seama, N., Isezaki, N., Fukuda, Y., 1996. Magnetic anomaly lineations and fracture zones deduced from vector magnetic anomalies in the West Enderby Basin. In: Storey, C., King, C., Livermore, R. (Eds.), *Weddell Sea Tectonics and Gondwana Breakup*. Geological Society of London, London, pp. 265–273. <https://doi.org/10.1144/GSL.SP.1996.108.01.19>.
- Olierook, H.K.H., Jiang, Q., Jourdan, F., Chiaradia, M., 2019. Greater Kerguelen large igneous province reveals no role for Kerguelen mantle plume in the continental breakup of eastern Gondwana. *Earth Planet. Sci. Lett.* 511, 244–255.
- Operto, S., Charvis, P., 1995. Kerguelen Plateau: a volcanic passive margin fragment? *Geology* 23, 137–140. [https://doi.org/10.1130/0091-7613\(1995\)023<0137:KPAVPM>2.3.CO;2](https://doi.org/10.1130/0091-7613(1995)023<0137:KPAVPM>2.3.CO;2).
- Operto, S., Charvis, P., 1996. Deep structure of the southern Kerguelen Plateau (southern Indian Ocean) from ocean bottom seismometer wide-angle seismic data. *J. Geophys. Res.* 101, 25077–25103. <https://doi.org/10.1029/96JB01758>.
- Pankhurst, R.J., Rapela, C.W., 1995. Production of Jurassic rhyolite by anatexis of the lower crust of Patagonia. *Earth Planet. Sci. Lett.* 134, 23–36. [https://doi.org/10.1016/0012-821X\(95\)00103-J](https://doi.org/10.1016/0012-821X(95)00103-J).
- Patriat, P., Segouin, J., 1988. Reconstruction of the Central Indian Ocean. *Tectonophysics* 155, 211–234. [https://doi.org/10.1016/0040-1951\(88\)90267-3](https://doi.org/10.1016/0040-1951(88)90267-3).
- Powell, C.M.A., Roots, S.R., Veivers, J.J., 1988. Pre-breakup continental extension in East Gondwanaland and the early opening of the eastern Indian Ocean. *Tectonophysics* 155, 261–283. [https://doi.org/10.1016/0040-1951\(88\)90269-7](https://doi.org/10.1016/0040-1951(88)90269-7).
- Ramana, M.V., Ramprasad, T., Desa, M., 2001. Seafloor spreading magnetic anomalies in the Enderby Basin, East Antarctica, *Earth Planet. Sci. Lett.* 191, 241–255. [https://doi.org/10.1016/S0012-821X\(01\)00413-7](https://doi.org/10.1016/S0012-821X(01)00413-7).

- Royer, J.Y., Coffin, M.F., 1992. Jurassic to Eocene plate tectonic reconstructions in the Kerguelen Plateau region. *Proc. Ocean Drill. Program Sci. Rep.* 120, 917–928. <https://doi.org/10.2973/odp.proc.sr.120.200.1992>.
- Sandwell, D.T., Müller, R.D., Smith, W.H.F., Garcia, E., Francis, R., 2014. New global marine gravity model from Cryo-Sat-2 and Jason-1 reveals buried tectonic structure. *Science* 346 (6205), 65–67. <https://doi.org/10.1126/science.1258213>.
- Stagg, H.M.J., Colwell, J.B., Dieren, N.G., O'Brien, P.E., Bernardel, G., Borissova, I., Brown, B.J., Ishirara, T., 2004. Geology of the continental margin of Enderby and MacRobertson Lands, East Antarctica: insights from a regional data set. *Mar. Geophys. Res.* 25, 183–219. <https://doi.org/10.1007/s11001-005-1316-1>.
- Talwani, M., Heitzler, J.R., 1964. Computation of magnetic anomalies caused by two dimensional structures of arbitrary shape. *Computers in the mineral industries, part 1: Stanford University publications. Geol. Sciences* 1, 464–480.
- Talwani, M., Worzel, J.L., Landisman, M., 1959. Rapid Gravity computations for Two-Dimensional Bodies with Application to the Mendocino Submarine Fracture Zone. *J. Geophys. Res.* 64, 49–59. <https://doi.org/10.1029/JZ064i001p00049>.
- Tewari, H.C., Kumar, P., 2003. Deep seismic sounding studies in India and its tectonic implications. *J. Virtual Explor.* 12, 30–54.
- Voss, M., Schmidt-Aursch, M.C., Jokat, W., 2009. Variations in magmatic processes along the East Greenland volcanic margin. *Geophys. J. Int.* 177 (2), 755–782. <https://doi.org/10.1111/j.1365-246X.2009.04077.x>.
- Weis, D., Ingle, S., Damasceno, D., Frey, F.A., Nicolaysen, K., Barling, J., Leg 183 Shipboard Scientific Party, 2001. Origin of continental components in Indian Ocean basalts: Evidence from Elan Bank (Kerguelen Plateau, ODP Leg 183, Site 1137). *Geology* 29, 147–150. [https://doi.org/10.1130/0091-7613\(2001\)029<0147:OOCII>2.0.CO;2](https://doi.org/10.1130/0091-7613(2001)029<0147:OOCII>2.0.CO;2).
- Wessel, P., Smith, W.H.F., Scharroo, R., Luis, J.F., Wobbe, F., 2013. Generic mapping tools : improved version released, EOS. *Trans. Am. Geophys. Union* 94, 409–410. <https://doi.org/10.1002/2013EO450001>.
- White, R.S., McKenzie, D., O'Nions, R.K., 1992. Oceanic crustal thickness from seismic measurements and rare earth element inversions. *J. Geophys. Res.* 97 (B13), 19683–19715. <https://doi.org/10.1029/92JB01749>.
- White, R., Smith, L., Roberts, A., P., A.F., Kuszniir, N.J., the rest of the iSIMM Team, 2008. Lower-crustal intrusion on the North Atlantic continental margin. *Nature* 452, 460–464. <https://doi.org/10.1038/nature06687>.
- Whittaker, J.M., Williams, S.E., Müller, R.D., 2013. Revised tectonic evolution of the Eastern Indian Ocean: Geochemistry. *Geophysics, Geosystem* 14, 1891–1909. <https://doi.org/10.1002/ggge.20120>.
- Williams, S.E., Whittaker, J.M., Granot, R., Müller, D.R., 2013. Early India-Australia spreading history revealed by newly detected Mesozoic magnetic anomalies in the Perth Abyssal Plain. *J. Geophys. Res. Solid Earth* 118, 1–10. <https://doi.org/10.1002/jgrb.50239>.
- Wobbe, F., Gohl, K., Chambord, A., Sutherland, R., 2012. Structure and breakup history of the rifted margin of West Antarctica in relation to Cretaceous separation from Zealandia and Bellingshausen plate motion. *Geochem. Geophys. Geosyst.* 13, Q04W12. <https://doi.org/10.1029/2011GC003742>.
- Xu, T., Zhang, Z.J., Liu, B.F., Chen, Y., Zhang, M.H., Tian, X.B., Xu, Y.G., Teng, J.W., 2015. Crustal velocity structure in the Emeishan large igneous province and evidence of the Permian mantle plume activity. *Sci. China Earth Sci.* 58, 1133–1147. <https://doi.org/10.1007/s11430-015-5094-6>.
- Zelt, C.A., Smith, R.B., 1992. Seismic traveltimes inversion for 2-D crustal velocity structure. *Geophys. J. Int.* 108, 16–34. <https://doi.org/10.1111/j.1365-246X.1992.tb00836.x>.